This document was prepared in conjunction with work accomplished under Contract No. DE-AC09-96SR18500 with the U.S. Department of Energy.

DISCLAIMER

The Interaction of Dissolved H with Internally Oxidized *Pd*-Rh Alloys.

D. Wang[(1)], J. D. Clewley[(1)], Ted B. Flanagan[(1)], R. Balasubramaniam[(2)], K. L. Shanahan[(3)]

(1) Chemistry Department and Materials Science Program, University of Vermont, Burlington VT 05405 USA

(2) Department of Materials and Metallurgical Engineering Indian Institute of Technology, Kanpur 208 016 India

(3) Westinghouse Savannah River Co., Aiken, SC 29802 USA

Abstract

Homogeneous fcc *Pd*-Rh alloys have been internally oxidized in the atmosphere at several temperatures from 1023 to 1123 K forming oxide precipitates within a Pd matrix. As shown from electron diffraction patterns of the internally oxidized $Pd_{0.97}Rh_{0.03}$ alloy, the oxide that forms is a mixed oxide, $PdRhO_2$. Internally oxidized *Pd*-Rh alloys can be reduced with H_2 (573 to 623 K) forming PdRh precipitates within a Pd matrix. This represents a way of segregating components of a substitutional solid solution binary alloy. The segregated alloy can be returned to the homogeneous *Pd*-Rh alloy by annealing at an elevated temperature and thus, in contrast to the internal oxidation of, e.g., *Pd*-Al alloys, the process can be readily reversed. The oxidation and (reduction + H_2O loss) were monitored from weight changes.

After internal oxidation/reduction "diagnostic" hydrogen isotherms (323 K) were measured to follow the extent of oxidation and to determine the extent of trapped H from the positive intercepts along the H/Pd axis in the dilute phase. The H capacities in the steeply rising hydride region of the H_2 isotherms for the internally oxidized alloys are smaller than for Pd unless the Pd in the PdRh precipitates is considered to be inactive for H_2 absorption for the calculation of H/Pd values.

In the two-phase region the absorption plateau pressures were significantly greater than for Pd-H, however, they were much closer to the Pd plateau p_{H2} than to the unoxidized *Pd*-Rh alloys. The desorption plateaux were very close to that of Pd-H for X_{Rh}=0.01 to 0.05 alloys and therefore it can be concluded that the matrix is pure Pd whose plateaux are affected by the presence of the precipitates.

The techniques of TEM, SEM and SANS (small angle neutron scattering) were employed to examine the alloys after internal oxidation and both before and after reduction. SANS confirmed directly that internal precipitates form from the internal oxidation and that they are rather large with an appreciable fraction having diameters greater than 100 nm.

Introduction

Binary *Pd*-M alloys containing small amounts of readily oxidizable solute metals such as M=Al, Mg, or Zr, can be internally oxidized to form essentially pure Pd matrices containing a second

phase of nano-sized oxide precipitates [1,2]. During internal oxidation Pd atoms are transported to the surface forming Pd nodules while vacancies are transported from the surface to the metal/oxide interface relieving the compressive stress which develops within the alloy due to the expanding metal oxide precipitates [3,4,5]. The Pd alloys that have been studied contain solutes that form very stable oxides [1].

Although Rh is usually considered to be a relatively noble metal, it will be demonstrated that Rh can be internally oxidized in *Pd*-Rh alloys. Pure Rh forms two oxides: RhO_2 and Rh_2O_3 depending on the temperature range [6] but it has recently been shown that the mixed oxide, $PdRhO_2$ forms from internal oxidation of *Pd*-Rh alloys [7]. The oxide precipitates which form should be relatively large compared to other internally oxidized solutes which have been investigated, e.g., MgO or Al_2O_3, since precipitate size increases as the *instability* of the oxide increases [8]. It may be possible to reduce the oxide precipitates with H_2 and, after reduction, the segregated alloy can be re-oxidized to reform the oxide precipitates; thus this may be a relatively versatile system where internal oxidation can be reversed.

A Pd-rich alloy-H system, like Pd-H itself, has a two solid phase co-existence region: (dilute + hydride) phases. According to the phase rule such a two-phase region should have a constant p_{H2} referred to as the plateau pressure; it increases with X_{Rh} in *Pd*-Rh alloys and the plateau breadth increases compared to Pd-H for $X_{Rh} \geq 0.10$.

After complete internal oxidation and reduction, a H_2 isotherm (323 K) of a *Pd*-Rh alloy should change to one with a lower plateau p_{H2} and a H capacity characteristic of pure Pd, demonstrating that Rh has been oxidized to precipitates within an essentially pure Pd matrix. Hydride formation, in contrast to hydrogen solution in the dilute phase of Pd-H, occurs by interface penetration and the abrupt volume expansion accompanying the hydride phase change causes dislocation formation and plastic deformation [9].

The chemical potential of dissolved H in Pd and in Pd-rich alloys can be readily measured from the equilibrium p_{H2}. This has been employed as a probe for metal/oxide interfaces in several internally oxidized *Pd*-M alloys where, e.g., M=Zr, Mg, Al [1, 10]. The initial deviations from the linear solubility relation reflect H trapping at the Pd/oxide interface. When these traps are filled [1], the H diffusion constant becomes comparable to its value in the dilute phase of Pd-H [1]. In this research, diagnostic H_2 isotherms will be used to help characterize a different type of internal interface, i.e., metal(Pd)/alloy(PdRh).

Experimental

Pd-Rh alloys were prepared by arc-melting the pure elements, annealing the buttons and rolling them into foil of dimensions about 2 cm x 0.3 cm x 110 μm. XRD patterns showed that the alloys were homogeneous fcc solid solutions. The internal oxidation was carried out in a tube furnace in the laboratory atmosphere. The percent oxidation was determined from the weight gain and/or the hydrogen absorption isotherm. The weight gain method was generally reliable to about ±5%.

The internally oxidized *Pd*-Rh alloys were reduced in H_2 generally at 10 bar at 573 K (or 653 K) and during the reduction the reaction volume was frequently evacuated in order to remove any

evolved H_2O. From the weight changes, only the total: (reduction + water loss) can be measured. The extent of (reduction + water loss) was often incomplete despite long periods of time. As long as the internally oxidized alloy had been exposed to H_2 (10 bar) at 573 K (or 653 K) for several hours, however, the subsequent H_2 isotherms showed no further signs of reduction whereas internally oxidized alloys, which had not been reduced, showed evidence of H_2O formation during H_2 solubility measurements. (Reduction + water loss) at 1 bar H_2 was not as efficient as 10 bar. For example, after exposures of an internally oxidized alloy to H_2 followed by evacuation, the (reduction + water loss) was about 70% at 10 bar and about 40% at 1 bar after several hours.

The changes introduced by internal oxidation were followed from diagnostic H_2 isotherms (323 K) measured before and after internal oxidation. They provide a convenient *in situ* method to follow internal oxidation and also to determine H segregation to the internal interfaces.

SEM was carried out at the IIT Kanpur (India) using a JEOL (JSM840A) SEM unit and elemental analysis was carried out by EMPA on a JEOL instrument. HREM (TEM) was carried out by Professor Y. Sakamoto at Nagasaki University (Japan). SANS measurements were performed at NIST by Dr. J. Barker.

Results and Discussion

Internal Oxidization of *Pd*-Rh Alloys.

The Pd-Rh alloy system has a miscibility gap below about 1173 K [11,12] and, according to the published phase diagrams, the Rh contents employed in this work should be outside of this gap at the internal oxidation temperatures, however, as a precaution to verify that the temperatures employed for internal oxidation did not cause any phase separation according to the miscibility gap, a homogeneous $Pd_{0.90}Rh_{0.10}$ alloy was heated *in vacuo* under typical conditions employed for internal oxidation, 3d at 1023 K. This composition and temperature are just outside of the miscibility gap boundary according to the literature [11,12]. After this treatment, no changes were found in the alloy's diagnostic H_2 isotherms (323 K) and therefore the miscibility gap cannot be a factor at the temperatures of internal oxidation employed. Although the temperature used for the H_2 diagnostic isotherms fall within the miscibility gap, this is not a problem because fcc *Pd*-Rh binary alloys are metastable for very long times at moderate temperatures [11].

Stoichiometry of Internal Rh Oxides.

The *Pd*-Rh alloys were weighed at various intervals to monitor the extent of internal oxidation; this is a reasonably accurate procedure because internal oxidation causes appreciable weight gains. After internal oxidation of the *Pd*-Rh alloys was apparently complete, the weight gains corresponded more closely to RhO_2 or $PdRhO_2$ rather than to Rh_2O_3 although the latter is reported to be more stable than RhO_2 in this temperature range [6]. A $Pd_{0.97}Rh_{0.03}$ alloy was internally oxidized at 1073 K for 120 h and, according to its weight gain, the oxide formed corresponded to a (O/Rh)=1.92 atom ratio. Under conditions where internal oxidation was expected to be complete, other internally oxidized alloys gave (O/Rh) ratios between 1.80 and 2.00. If Rh_2O_3 were to be formed, the ratio would be a maximum of 1.5. The internal oxidation was relatively slow because

the temperatures could not be raised above ~1200 K because above this, the equilibrium p_{O2} over the oxide exceeds that in the atmosphere.

Optical Microscopic Observations, SEM, EDAX, SANS.

Optical microscopic observations of the surface of the internally oxidized $Pd_{0.90}Rh_{0.10}$ foils did not reveal very much surface structure because of a thin oxide layer on the surface presumably due to some surface oxidation of Pd; after the internally oxidized/reduced alloy was cycled through the hydride phase at 323 K, an intergranular network of cracks could be seen. Such a crack network cannot be seen after cycling Pd.

SEM micrographs were taken of an internally oxidized $Pd_{0.97}Rh_{0.03}$ alloy (1073 K) before and after reduction. Before reduction, it appeared as if some of the surface was covered with a thin layer and, where this had peeled off, a few intergranular cracks could be seen and nodules of pure Pd were detected and verified by EDAX. Such nodules are apparent for internally oxidized *Pd*-Al alloys [5] which is consistent with the occurrence of internal oxidation [3]. Extensive and large intergranular cracks were apparent after reduction as seen in Figure 1. Although not visible in Figure 1, blisters could be seen on the surface after reduction which were mainly intergranular and must be associated with water vapor formation from the reduction.

Many of the X-ray peaks for Pd and Rh are close to each other making quantitative analysis by EDAX difficult, but not impossible, since several peaks do not overlap. After reduction there were no surface regions which appeared to be only Rh but some, which were mainly near boundaries rather than within grains, were richer in Rh while others appeared to be pure Pd. This is consistent with the presence of PdRh precipitates within a Pd matrix.

SANS (small angle neutron scattering) was carried out at the National Institute of Standards and Technology by Dr. J. Barker. SANS patterns were determined for the internally oxidized (1073 K) $Pd_{0.97}Rh_{0.03}$ and $Pd_{0.95}Rh_{0.05}$ alloys and the scattering intensity of the latter was found to be greater than the former. From the SANS curves it can be deduced that an appreciable fraction of the precipitates had diameters greater than 100 nm which is consistent with the relative instability of the oxide which allows its dissociation and growth during internal oxidation [8].

An unexpected result from SANS was that the neutron scattering intensity was greater from an internally oxidized $Pd_{0.95}Rh_{0.05}$ alloy which had been reduced than for the unreduced form which is contrary to expectations since there is little difference between the scattering length densities of PdRh, i.e., the reduced precipitates, and the Pd matrix. It is probable that H_2O occupying a void volume adjacent to the precipitates after reduction leads to the observed increased scattering intensity because a brief heating of the reduced alloy to 973 K markedly reduced its scattering intensity, presumably due to water loss.

TEM and Electron Diffraction of Internally Oxidized *Pd*-Rh Alloys.

TEM (×300k) revealed some large precipitates after internal oxidation, e.g., 300 nm, which is consistent with the SANS results. Moiré fringes are apparent between the oxide and the Pd matrix

(Fig. 2) which indicates that there are two overlapping parallel planes in the two structures with different lattice parameters. Compared to internal oxidation of *Pd*-Al alloys, the Pd matrix of the internally oxidized $Pd_{0.97}Rh_{0.03}$ alloy has more irregularities, i.e., pits and dark appearing material (Fig. 2). The matrix of an internally oxidized $Pd_{0.98}Ni_{0.02}$ alloy has a similar appearance [13].

After reduction, the large oxide crystallites break up into smaller ones of various sizes with no orientational relationship to the original large crystallites (Fig. 2). Some Moiré fringes were observed which extended for only small distances and tended to be wavy and irregular indicating dislocations and a semi-coherent interface in those places. There was no obvious indication of any void volume adjacent to the crystallites but these may be so small that they are difficult to see even at ×300k magnification.

Electron diffraction patterns of the internally oxidized $Pd_{0.97}Rh_{0.03}$ alloy clearly revealed, in addition to the fcc Pd lattice, a weak set of reflections from the oxide. The oxide did not index according to either RhO_2 or Rh_2O_3 but was consistent with the structure of $PdRhO_2$ [14] as noted elsewhere [15]. Such mixed oxides resulting from internal oxidation have been hypothesized before on the basis of the weight changes rather than by identification from diffraction patterns. In the present case the weight gains are the same for RhO_2 and $PdRhO_2$, and it would therefore be impossible decide between them on this basis. The mixed oxide, $PdRhO_2$ has an HCP structure and may form instead of a pure Rh oxide because of its better orientational relationship with the Pd lattice. After reduction, the reflections from the oxide were no longer visible indicating nearly complete reduction.

Rates of Internal Oxidation of *Pd*-Rh Alloys.

There should be a linear ξ versus $\sqrt{t}$ relationship where ξ is the penetration of the internal oxidation interface [8]. Some data for the internal oxidation of a $Pd_{0.97}Rh_{0.03}$ alloy at 1098 K are shown in Figure 3 where the % internal oxidation has been plotted instead of ξ. These quantities are directly proportional for a thin foil specimen since the large foil dimensions remain nearly constant during internal oxidation. Aside from the initial and final ~10% of the internal oxidation (Fig. 3), the relation is reasonably linear. The initial deviations from linearity may be due to difficulties in nucleation of $PdRhO_2$ because of its relatively small $|\Delta G^o_f|$ [8].

The rate of re-internal oxidation of a $Pd_{0.97}Rh_{0.03}$ alloy, which had not been cycled but had been previously segregated into PdRh precipitates within the Pd matrix by reduction of an internally oxidized *Pd*-Rh alloy, was faster than the internal oxidation of the original, homogeneous alloy. This suggests that transport of oxygen in the composite must be facilitated by the microcracks seen after internal oxidation and reduction, i.e., O_2 is transported *via* cracks where it dissociates on the crack walls and diffuses into the bulk. This increases the rate of internal oxidation because of the shorter oxygen diffusion paths.

Reduction of Internally Oxidized *Pd*-Rh Alloys.

The free energy change for the reduction of $PdRhO_2$ with H_2 must be quite negative since the reduction of RhO_2 is very negative and the two oxides must have similar stabilities because they decompose in the atmosphere at similar temperatures. The internally oxidized alloys were found to

undergo (reduction + water loss) in H_2 at 10 bar in the temperature range from 573 K to 653 K, however, it was generally incomplete. For example, after about 48 h the average (reduction + water loss) for five samples of the internally oxidized $Pd_{0.90}Rh_{0.10}$ alloy was 80% and for two reductions of the internally oxidized $Pd_{0.95}Rh_{0.05}$ alloy it was less than this.

It is possible that reduction with H_2 takes place readily at 573 K to 653 K but is not reflected by the weight loss because of the H_2O that remains in the solid. If this is the case, heating the internally oxidized/reduced alloy at the appropriate temperature should expel the water, giving the weight change corresponds to complete (reduction + water loss). The following experiment was carried out to test this. An internally oxidized $Pd_{0.90}Rh_{0.10}$ alloy was reduced at 623 K (10 bar) to 86% (reduction + water loss). Separate foils of this alloy were then heated *in vacuo* at 873 K, 923 K and 973 K for 1 h periods and from the weight losses, 94% (reduction + water loss) took place at 873 K (1 h) and not much change occurred after an additional 3 h heating. Another foil was heated *in vacuo* for 2 h at 923 K leading to a 95.1 % (reduction + water loss) and after heating another foil for 2 h at 973 K, the (reduction + water loss) was 100%. A 100% loss at 973 K was also found in a repeat determination with another foil. This shows that reduction had occurred completely at the lower temperatures but all of the water did not escape until heated to higher temperatures. After reduction, the oxide precipitate shrinks, providing a volume for the water molecules. At high temperatures the high vapor pressures of water which develop in the small volumes leads to microcracking and water escape. This is similar to the reduction of Cu_2O by H_2 within Cu as discussed by Fast [16]. Blisters observed here by SEM can be taken as evidence of water formation and escape [8].

An isotherm for an *unreduced* internally oxidized $Pd_{0.90}Rh_{0.10}$ alloy was measured at 323 K and data were taken so that the alloy was rapidly within the plateau region. The plateau pressure for hydride formation was somewhat lower than for the internally oxidized/reduced alloy but closer it than to the p_f of Pd-H. As will be seen below the plateau pressure for hydride formation, p_f, is greater for the internally oxidized *Pd*-Rh alloys than for Pd-H but p_d is similar. Therefore increased p_f values are found whether or not the internally oxidized alloy has been completely reduced.

The percent unreduced oxide can be determined from the sample weights before and after internal oxidation and after heating *in vacuo* at 973 K for 12 h which has been shown above to be sufficient to remove all of the trapped water. The weight changes were measured after an isotherm measurement at 323 K with an unreduced $Pd_{0.90}Rh_{0.10}$ alloy that included storage of the alloy at 0.6 bar p_{H2} (in the hydride phase) for 12 h. About 67% reduction took place during the isotherm measurement at 323 K over a total period of 18 h. After this isotherm measurement, about 35% of the water was lost and about 32% remained within the alloy.

During the isotherm measurement a value of r=0.705 was measured at 0.30 bar from the p_{H2} changes instead of 0.645 characteristic of Pd-H at this p_{H2} indicating about 15% reduction occurred during 6 h period of the measurements. Reduction causes the loss of H_2 if the water is retained in the solid. In the steeply rising portion of the isotherm beyond the end of the plateau it was apparent that further reduction took place and, after 12 h at ~0.6 bar, the apparent H content of the alloy increased from *r*=0.705 to 0.88 which represents an additional 44% reduction or an estimated 59% total during the internal oxidation (323 K) from the p_{H2} changes as compared to 67% from the

weight changes. The latter should be more accurate. In any case, complete reduction does not occur at 323 K during the isotherm measurements which is somewhat surprising.

Kinetics of Hydrogen Absorption by Internally Oxidized/Reduced Alloys.

A few remarks about the kinetics of H_2 absorption should be made because greatly enhanced rates were observed for internally oxidized *Pd*-Al alloys [17] as compared to Pd. During absorption along the two phase, plateau region (323 K), the pH2 falls with time as shown in Figure 4 for an internally oxidized *Pd*-Rh alloy; this is much faster than for Pd foil but somewhat slower than for internally oxidized *Pd*-Al alloys. After cycling through the hydride phase, the rate of the internally oxidized $Pd_{0.97}Rh_{0.03}$ alloy appeared to be slightly faster than the initial one after internal oxidation/reduction.

Isotherms for Unoxidized *Pd*-Rh Alloys.

Isotherms are available in the literature for some homogeneous *Pd*-Rh alloys [18,19] but not for several values of $X_{Rh} \leq 0.05$ needed in this research. For this reason dilute phase H_2 solubilities (323 K) were determined for the unoxidized, homogeneous *Pd*-Rh alloys (Fig. 5) where it can be seen that the H_2 solubility at a given p_{H2} decreases with increase of X_{Rh}. All of the solubilities intersect the origin according to the ideal solubility law as $r \rightarrow 0$, $r = K_s p_{H2}^{1/2}$, where K_s is a constant [20].

The plateau H_2 pressures increase markedly with X_{Rh} as shown in Figure 6 (323 K) and even for X_{Rh} as small as 0.01, the plateau is significantly greater than for Pd-H. The H capacity decreases slightly from that of Pd-H with increase of X_{Rh} and then increases for $X_{Rh} \geq 0.10$. *Pd*-Rh alloys are unique because they are the only substitutional Pd-rich alloys where the H capacities increase with atom fraction of solute in the moderate p_{H2} range. (*Pd*-Ni alloys have plateaux which decrease and then increase with X_M like *Pd*-Rh alloys but even at about 100 bar the plateau is only about as wide as that of Pd [21]).

Isotherms for Internally Oxidized *Pd*-Rh Alloys.

Dilute Phase Hydrogen Solubilities for Uncycled Alloys

Dilute phase H_2 solubilities (323 K) for a series of internally oxidized/reduced *Pd*-Rh alloys have been measured and are described below starting with the lowest Rh content. H_2 solubilities (323 K) were determined *after each* of the treatments carried out in sequence: *i*) internal oxidation/reduction and evacuation at 573 K, *ii*) evacuation at 323 K, *iii*) cycling through the hydride phase transition (323 K) and evacuation (323 K). After treatment (*i*) the alloy is H free whereas after treatment (*ii*) there will be some strongly held H which is not removed by evacuation at 323 K. The H/Pd ratios in the Figures to be shown have been computed excluding Pd in the precipitate phase because PdRh absorbs significant H_2 only at several thousand atmospheres at 323 K [22]. Unless otherwise specified, this, and the remaining alloys, were internally oxidized/reduced under the same conditions as the $Pd_{0.99}Rh_{0.01}$ alloy described immediately below.

Although treatments *i-iii* were carried out for each alloy, the results will not be described for each because of their similarity. Some results for H_2 solubilities after annealing the internally oxidized alloys at higher temperatures will also be described for the internally oxidized $Pd_{0.90}Rh_{0.10}$ alloy.

$Pd_{0.99}Rh_{0.01}$ The internally oxidized (1073 K, 3d)/reduced (573 K, 10 bar, 3 h) $Pd_{0.99}Rh_{0.01}$ alloy has a very similar dilute phase solubility as Pd but, instead of intersecting the origin, there is a small intercept along the *r*-axis of about H/Pd=*r*=0.0005 and therefore data do not follow the ideal solubility law, $r = K_s p_{H2}^{1/2}$, as $r \rightarrow 0$. The positive intercept indicates the presence of trapping sites more energetic for H occupation than normal octahedral interstices.

$Pd_{0.97}Rh_{0.03}$ Data for this internally oxidized/reduced alloy $Pd_{0.97}Rh_{0.03}$ intersect the *r* axis at about 0.0013 (Fig. 7) indicating that there are more strong traps than for the internally oxidized $Pd_{0.99}Rh_{0.01}$ alloy. The intercept is somewhat smaller than that observed for an internally oxidized $Pd_{0.97}Al_{0.03}$ alloy [13]. The slope of the solubility plot is just slightly steeper than that for Pd-H but very different from the homogeneous alloy (Fig. 5) demonstrating that the matrix is essentially pure Pd after internal oxidation.

$Pd_{0.95}Rh_{0.05}$ Dilute phase isotherms for this internally oxidized /reduced alloy are shown in Figure 8 where again there is a positive intercept along the H/M=*r* axis, 0.0015, and the dilute phase solubility curve, $p_{H2}^{1/2}$ against *r*, is otherwise similar to Pd-H. For the repeat measurement there is a small, but measurable intercept indicating that about half of the trapped H can be removed by evacuation (323 K).

$Pd_{0.90}Rh_{0.10}$ Dilute phase isotherms for the internally oxidized/reduced $Pd_{0.90}Rh_{0.10}$ alloy are shown in Figure 9. The intercept is 0.003 and, after evacuation for 2 h at 323 K, a repeat measurement gives an intercept of 0.0015. This proves that the H traps are not as deep as for internally oxidized $Pd_{0.97}Al_{0.03}$ where H cannot be removed until temperatures $\geq$573 K are reached [1]. Another $Pd_{0.90}Rh_{0.10}$ alloy was internally oxidized at a lower temperature, 1023 K (3 d), and then reduced; its H_2 solubility and intercept are similar to those in Figure 9. A $Pd_{0.90}Rh_{0.10}$ alloy was internally oxidized at a slightly higher temperature, 1123 K (72 h), and its intercept along the *r*=H/M axis was also *r*=0.003.

Dilute phase solubilities for the internally oxidized/reduced $Pd_{0.90}Rh_{0.10}$ alloy shown in Figure 9 were determined (323 K) after each of the following annealing/evacuation treatments carried out in sequence: 353 K, 373 K, 403 K, 443 K, 473 K and 503 K for 2 h periods (Fig. 9). The amount of H removed by the annealing/evacuation can be determined from the H_2 solubility, i.e., the intercept, after these annealing treatments, e.g., if all of the H is removed, it can all be replaced so the intercept would be *r*=0.003 (Fig. 9), but if only half can be removed, then it can only be replaced up to *r*=0.0015. It can be seen that slightly more H is removed after each higher annealing temperature and, after annealing/evacuation at 503 K, it is all removed. The fact that small amounts are removed after each increment of temperature indicates that there is a spectrum of trapping energies.

The initial solubility for another internally oxidized $Pd_{0.90}Rh_{0.10}$ alloy is shown in Figure 10. Repeat solubility measurements after evacuation at 323 K for 2 h and 12 h at 323 K gave the same result as the 2 h evacuation (323 K) shown in Figure 9 where the intercept is about 0.0015. The

good reproducibility of the amount of dilute phase trapping demonstrates that their number is independent of the precise degree of (reduction + water loss) which suggests that the trapping is due to an invariant property such as the total Pd/PdRh interfacial area.

The internally oxidized $Pd_{0.90}Rh_{0.10}$ alloy shown in Figure 10 was then annealed/evacuated at a series of higher temperatures than used for the alloy shown in Figure 9. The results are more complicated than those in Figure 9 because the H *and* some traps are removed by the higher temperature annealing/evacuations. It was shown in Figure 9 that all of the H can be removed at $\geq$503 K and therefore the smaller intercepts found after higher temperature annealing/evacuation (Fig. 10) indicate that H can no longer be trapped to the same extent as the initial trapping because some of the traps have been eliminated. After the initial solubility measurements (323 K), the internally oxidized alloy was evacuated at 673 K for 2 h and the intercept was then slightly smaller than the initial one indicating that besides the removal of H_2, some traps are eliminated (Fig. 10). Evacuation at 773 K for 2 h eliminates about half of the trapping sites and evacuation at 873 K for 2 h eliminates all of them. It should be noted that the shapes of the H_2 solubility relations are basically unchanged from Pd-H (Fig. 10) indicating that there is negligible interdiffusion between Rh in the precipitates and the Pd matrix. Thus the traps are removed without eliminating the PdRh precipitates and the accompanying Pd/PdRh interfaces.

For internally oxidized *Pd*-Al alloys annealing/evacuation at elevated temperatures removes the strong trapping sites which are, according to [1], O atoms at the interface. In the present case trapping cannot occur because of O at the interface and, perhaps, a defect such as vacancies adjacent to the interface are traps which can be eliminated by annealing internally oxidized/reduced *Pd*-Rh alloys.

Another $Pd_{0.90}Rh_{0.10}$ alloy was internally oxidized for 24 h at 1273 K and its H_2 solubility was very similar to that of the unoxidized alloy intersecting the origin (Fig. 10). Consistent with this was its negligible weight gain indicating that internal oxidation does not take place at 1273 K because the dissociation pressure of the oxide must be greater than the surrounding O_2 pressure.

After allowing for the strongly trapped H, internally oxidized *Pd*-Rh alloys were found to have similar dilute phase H_2 solubilities as Pd differing from internally oxidized *Pd*-Al alloys [10] where enhanced solubilities were found which were attributed to a tensile stress field (thermal residual stress) resulting from the effect of different thermal coefficients of expansion of the matrix and alumina when the alloy is cooled from the internal oxidation temperature to room temperature [10]. The *Pd*-Rh alloys were reduced after internal oxidation and therefore any stress fields from thermal residual stress would be relaxed.

Dilute Phase Hydrogen Solubilities for Cycled Alloys.

After the $Pd_{0.97}Rh_{0.03}$ alloy was hydrided and dehydrided (cycled) at 323 K and evacuated, its solubility was re-determined (323 K) (Fig. 7) and the *r* intercept is about the same as for the initially internally oxidized alloy (Fig. 7) which is of considerable interest. As expected, the dilute phase solubility is enhanced after cycling due to H-dislocation interaction are the H_2 solubilities at a given p_{H2} after and before cycling, is slightly greater than that for cycled pure Pd and the enhancement increases with X_{Rh}. The dislocation density introduced by cycling is not as large as

found for a cycled, internally oxidized (1073 K) $Pd_{0.97}Al_{0.03}$ alloy where the small and closely spaced alumina precipitates cause a marked increase in dislocation densities [24].

An internally oxidized $Pd_{0.95}Rh_{0.05}$ alloy was also cycled and the solubility data re-measured and, as expected, there is a solubility enhancement. The intercept is also the same for this alloy as for the initial solubility after internal oxidation/reduction (Fig. 8). When the solubility was re-measured for the cycled internally oxidized alloy after evacuation at 323 K (2 h), its intercept was unchanged.

An internally oxidized $Pd_{0.90}Rh_{0.10}$ alloy was annealed at 873 K for 20 h and its dilute phase solubility almost intersects the origin indicating elimination of most all the traps just as the 2 h annealing at 873 K eliminated them (Fig. 10). The solubility relationship is slightly steeper than for Pd-H indicating that a very small amount of Rh may have diffused into the Pd matrix. If this alloy is then cycled and evacuated (323 K), its intercept recovers and returns to the initial value found after internal oxidation showing that a Pd/PdRh interface is still extant and the traps have been regenerated. The same behavior has also been found for internally oxidized *Pd*-Al alloys [13]. The trap regeneration must be related to the interaction of dislocations, created during cycling, with the precipitates. Perhaps the traps are vacancies adjacent to the interface and are regenerated by the dislocations. It should be recalled that cycling pure Pd or precipitate-free alloys does not lead to a significant intercept.

Another internally oxidized/reduced $Pd_{0.90}Rh_{0.10}$ alloy was annealed at 973 K for 20 h and its dilute solubility relation was found to be steeper than for Pd-H approaching that for an unoxidized $Pd_{0.97}Rh_{0.03}$ alloy, indicating significant metal atom interdiffusion has occurred. After cycling this alloy, its H_2 solubility had a small intercept, r=0.0006. The H_2 solubility for an internally oxidized $Pd_{0.90}Rh_{0.10}$ alloy, which was annealed at 1073 K, and then cycled, intersected the origin. These results indicate that significant interdiffusion occurs during annealing at 973 K but not at 873 K because the trapping sites cannot be regenerated by cycling after the former.

Complete Isotherms for Internally Oxidized *Pd*-Rh Alloys.

The isotherm for the internally oxidized/reduced $Pd_{0.99}Rh_{0.01}$ alloy has a p_d almost identical to that of Pd-H but p_f is somewhat greater than that for Pd-H. There is no supersaturation as for annealed Pd [25,26].

Figure 11 shows H_2 isotherms (323 K) for the $Pd_{0.97}Rh_{0.03}$ alloy before and after internal oxidation/reduction where it can be seen that the absorption plateau p_{H2} is greater than for Pd-H and, because the desorption plateau does not change much, hysteresis is greater. There is supersaturation of the dilute phase before, but not after, internal oxidation. The limiting H capacity is very similar to Pd-H after internal oxidation again calculating H/Pd by excluding the Pd in the PdRh precipitates.

Figure 12 shows H_2 isotherms for the $Pd_{0.95}Rh_{0.05}$ alloy before and after internal oxidation/reduction. The increase of the absorption plateau p_{H2} relative to Pd-H is similar to that for the $Pd_{0.97}Rh_{0.03}$ alloy (Fig. 11); for the second cycle, the absorption plateau p_{H2} is slightly lower than the initial one but still greater than that for Pd-H. The H capacities are similar to Pd-H. There is supersaturation before, but not after, internal oxidation. Supersaturation disappears after internal

oxidation because there are enough imperfections, e.g., precipitates, for nucleation not to be a problem.

Figure 13 shows complete isotherms for the internally oxidized/reduced $Pd_{0.90}Rh_{0.10}$ alloy where *both* plateau pressures increase causing hysteresis to remain about the same as for the other internally oxidized alloys (Figs. 11, 12). (The isotherm for the well-annealed $Pd_{0.90}Rh_{0.10}$ alloy is not shown in Figure 13 because its plateau pressures are too great for the scale of the p_{H2} axis). Another $Pd_{0.90}Rh_{0.10}$ alloy, which had been completely internally oxidized and reduced, had similar plateau changes with respect to Pd-H as those shown in Figure 13.

An isotherm for a $Pd_{0.90}Rh_{0.10}$ alloy which was heated in the atmosphere at 1273 K is shown in Figure 6 where it can be seen that it is similar to an unoxidized alloy except that its hysteresis is slightly greater and there is more sloping of the desorption plateau. Even though no internal oxidation occurs at this temperature, microstructural changes have taken place because, if only annealing had occurred, the plateaux would be relatively horizontal.

It has been found here that annealing the internally oxidized $Pd_{0.90}Rh_{0.10}$ alloy at 873 K for 20 h causes p_f to increase further, in comparison to an unannealed internally oxidized $Pd_{0.90}Rh_{0.10}$ alloy, and also causes the capacity to decrease but it does not affect p_d (Fig. 13). This experiment was repeated with another internally oxidized $Pd_{0.90}Rh_{0.10}$ alloy with a very similar increase of p_f and decrease in capacity. The capacity decrease may be due to diffusion of some Rh into the matrix phase, however, the decrease is the same for 2 or 20 h anneals which would not normally be expected for diffusion. The solubility results in the dilute phase after internal oxidation and annealing at 873 K indicate that little intermetal diffusion occurs after 2 h annealing. This indicates that the capacity decrease may not be due to interdiffusion.

After similar annealing at 873 K of internally oxidized $Pd_{0.97}Rh_{0.03}$ and $Pd_{0.95}Rh_{0.05}$ alloys there were no effects on either the plateau pressures or the capacities.

The increased absorption plateau pressures for the internally oxidized *Pd*-Rh alloys, i.e., increased hysteresis, compared to Pd-H cannot be due to some Rh in the Pd matrix because the decomposition plateau is the same as for Pd-H. Since the detailed origin of hysteresis in these metal-H systems is unknown, it is difficult to speculate about the reason for the increased p_f values relative to Pd-H. It is obviously related to the presence of the precipitates. Essentially the same p_f was observed for the unreduced as for the reduced internally oxidized $Pd_{0.90}Rh_{0.10}$ alloy. Hysteresis is believed to be due to entropy production occurring during the interface movement and this is greater in the presence of the large precipitates.

Hysteresis Scans for Internally Oxidized *Pd*-Rh Alloys

A feature of hysteresis is that scans can be carried out from one branch to the other within the hysteresis gap [27]. Thus desorption scans carried out from the absorption plateau, p_f, reach the desorption plateau, p_d, when sufficient H_2 has been desorbed and *vice versa*. For the internally oxidized *Pd*-Rh alloys absorption scans were carried out from the desorption plateau. If the p_f at the end of the scan is close to the plateau p_f for Pd-H, it can be concluded that the matrix must be pure Pd, i.e., the increased plateau p_f values after internal oxidation cannot be due to small amounts

of Rh within the Pd. Two absorption scans for an internally oxidized $Pd_{0.97}Rh_{0.03}$ alloy are shown in Figure 14; the initial plateau pressures are slightly greater than shown in Figure 11. The first scan reaches the sloping absorption plateau at about the value corresponding to a sloping Pd-H plateau and the second scan also reaches a similar p_f, thus the scans do not reach a p_f characteristic of the internally oxidized alloy but one corresponding to Pd-H. After complete evacuation, another absorption isotherm agreed almost exactly with the first one for the annealed internally oxidized alloy.

An isotherm (323 K) for the internally oxidized $Pd_{0.90}Rh_{0.10}$ alloy is shown in Figure 15 where p_f is somewhat greater than for the internally oxidized $Pd_{0.97}Rh_{0.03}$ alloy. The scans also have changes of slope at the absorption plateau of Pd-H (Fig. 15) and they continue sloping to about the same extent as for the internally oxidized $Pd_{0.97}Rh_{0.03}$ alloy again showing that the matrix in the internally oxidized alloy is essentially pure Pd and not a solid solution of Pd and a small amount of Rh.

Several results such as the scan behavior and the values of p_d after internal oxidation, suggest that Rh in the Pd matrix cannot account for the increased plateau pressures, p_f, and another explanation must be sought. There can be no long-range stresses in the internally oxidized alloys because the dilute phase solubility is unaffected, i.e., it is basically the same as for Pd-H. Stress may develop during the hydriding process due to the presence of the PdRh precipitates. It is surprising, however, why relatively large PdRh precipitates should cause higher p_f values; internally oxidized *Pd*-Al alloys, where the oxide precipitates are smaller and closely spaced and interact strongly with dislocations, have the same initial p_f after internal oxidation as Pd-H. The dislocations involved with cycling may cut through the PdRh precipitates whereas they must bow around the alumina precipitates in internally oxidized *Pd*-Al alloys and perhaps this plays a role in determining pf.

Further H_2 scanning experiments were carried out with the internally oxidized $Pd_{0.90}Rh_{0.10}$ alloy after annealing at 873 K for 20 h. The isotherm (323 K) confirms the earlier, interesting result that annealing causes a significantly greater p_f and a reduced capacity compared to before annealing (Fig. 16). The scans for this annealed alloy also show a change of slope at the p_f of Pd-H and then the p_{H2} values increase close to that for the unannealed internally oxidized $Pd_{0.90}Rh_{0.10}$ alloy. After the absorption scan reached the single hydride phase, its capacity was found to be the same as the initial capacity after annealing. The desorption isotherm was the same as for the other internally oxidized $Pd_{0.90}Rh_{0.10}$ alloys.

Dilute Phase Intercepts along the *r*-Axis

Positive intercepts along the *r*-axis observed for the initial H_2 absorption are caused by trapping at energetic sites created by internal oxidation/reduction of the *Pd*-Rh alloys which increase nearly linearly with X_{Rh}. The number of traps are of the same order of magnitude as for several other internally oxidized, but not reduced, *Pd*-M alloys, M=Al, Ni, Y, i.e., r=0.0005 to 0.004 [13], suggesting that H is trapped at or near the interfaces despite differences in precipitate size, oxidation state and orientational relationships to the matrices. As noted above, positive intercepts observed for internally oxidized *Pd*-M alloys have been attributed to trapping by O at the Pd/oxide interfaces, e.g., Pd/Al_2O_3 and Pd/MgO [1]. There must be different traps for internally oxidized/reduced *Pd*-Rh alloys. The binding is weaker for the internally oxidized/reduced *Pd*-Rh alloys than for internally oxidized *Pd*-Al alloys because some H can be removed from the former,

but not the latter, by evacuation at 323 K and all of the H can be removed at 503 K whereas trapped H is not removed until 573 K for internally oxidized *Pd*-Al alloys [13].

There should be some solute trapping at all internal interfaces because of differences in surface tensions of the two phases in contact as described by the Gibbs adsorption isotherm [28]. Seidman and coworkers [29,30] have discussed the segregation of Ag to Cu/MgO interfaces at elevated temperatures using the Gibbs equation. Atomistic Monte Carlo simulations, e.g., [31], indicate that segregation is not limited to a single layer at the interface but a whole spectrum of segregation sites may exist. Such a non-specific segregation of H to the Pd/PdRh interfaces may take place in the internally oxidized/reduced *Pd*-Rh alloys.

After cycling, the intercepts are the same as after internal oxidation (Fig. 7) but the trapped H is not held as strongly, e.g., it can *all* be removed by evacuation at 323 K. It should be emphasized that after cycling either Pd (323 K) or the unoxidized alloys, their solubility relationships, despite H-dislocation solubility enhancements, closely intersect the origin. The abrupt volume expansion and contraction accompanying cycling requires extensive dislocation formation which weakens the bonding of the trapped H for both internally oxidized *Pd*-Al and *Pd*-Rh alloys, allowing it to be removed by evacuation (323 K). The traps in the internally oxidized *Pd*-Rh alloys can be eliminated by annealing at 873 K but are regenerated by cycling due to dislocation interaction with the precipitates.

Conclusions

Interesting findings in the research are: *i*) H trapping at PdRh/Pd interfaces characterized by positive intercepts in the dilute solubility phase, *ii*) after traps in the internally oxidized alloys have been eliminated by annealing at 873 K, they are regenerated by cycling (323 K), *iii*) greater plateau pressures for absorption, p_f, and greater hysteresis after internal oxidation as compared to Pd-H, *iv*) segregation of an homogeneous binary alloy into Pd and PdRh precipitates *via* internal oxidation/reduction and the return to the homogeneous state by annealing at 1173 K.

It has been shown that homogeneous Cu-Ni (5 at %) alloys can be segregated into Ni precipitates within a Cu matrix by internal oxidation/reduction [32]. Only very thin samples of these alloys can be employed because a $T \geq 773$ K is needed for reduction and which takes place faster in thin samples where the NiO precipitates are closer to the reducing agent, CO, at the surface than in thicker ones where the reduction times needed are so long that metal interdiffusion can take occur.

Pd-Rh alloys can be separated by internal oxidation followed by reduction by H_2 into two phases: pure Pd and PdRh precipitates. The process can be reversed by annealing the Pd/PdRh composite at a sufficiently high temperature to reform the homogeneous alloy, which can then be re-internally oxidized. Reduction *via* H has an advantage compared to reduction by other species because the precipitates within the bulk are quite accessible to dissolved H and the reduction takes place at relatively low temperature where interdiffusion is not a problem. A disadvantage of the *Pd*-Rh alloys is that the precipitate formed is not pure Rh but PdRh.

Acknowledgements

TBF and KLS acknowledge Westinghouse Savannah River Corporation for partial financial support of this research under DOE contract number DE-AC09-88SR18035. Dr. J. Barker is thanked for the SANS measurements and Professor Y. Sakamoto for carrying out HREM.

References

[1] X. Huang, W. Mader, R. Kirchheim, *Acta metall. mater.*, **39** (1991) 893.

[2] H. Noh, T. Flanagan, R. Balasubramaniam, J. Eastman, *Scripta Met. Mat.*, **34** (1996) 863.

[3] J. Mackert, R. Ringle, C. Fairhurst, *J. Dent. Res.*, **62** (1983) 1229.

[4] S. Guruswamy, S. Park, J. Hirth, R. Rapp, *Oxidation of Metals*, **26** (1986) 77.

[5] R. Balasubramaniam, R. Kirchheim, D. Wang, T. Flanagan, *J. Alloys Compounds*, **293-295** (1999) 517.

[6] E. Fromm, E. Gebhardt, *Gase in Metallen*, Springer-Verlag, Berlin (1976).

[7] D. Wang, T. Flanagan, R. Balasubramaniam, Y. Sakamoto, *Scripta Mat.*, **43** (2000) 685.

[8] J. Meijering, in *Advances in Materials Research*, H. Herman, ed., Wiley, New York, **5** (1971) p. 1.

[9] J. Lynch, J. Clewley, T. Curran, T. Flanagan, *J. Less-Common Mets.*, **55** (1973) 153.

[10] R. Balasubramaniam, H. Noh, T. Flanagan, Y. Sakamoto, *Acta Met. Mat.*, **45** (1997) 1725.

[11] E. Raub, H. Beeskow, D. Menzel, *Z. Metallkd.*, **50** (1959) 426.

[12] J. Shield, R. Williams, *Scr. Metall.*, **21** (1987) 1475.

[13] D. Wang, T. Flanagan, R. Balasubramaniam, *to be published*.

[14] R. Shannon, D. Rogers, C. Prewitt, *Inorg. Chem.*, **10** (1971) 713.

[15] R. Balasubramaniam, D. Wang, T. Flanagan, K. Shanahan, *Physical Chemistry Chemical Physics*, **2** (2000) 4976.

[16] J. Fast, *Interaction of Metals and Gases, Vol. 1*, Academic Press, N. Y. (1965).

[17] D. Wang, R. Balasubramaniam, T. Flanagan, K. Shanahan, *J. Alloys Compounds*, **298** (2000) 261.

[18] H. Noh, W. Luo, T. Flanagan, *J. Alloys and Compounds*, **196** (1993) 7.

[19] Y. Sakamoto, Y. Haraguch, M. Ura, F. Chen, *Ber. Bunsenges. Phys. Chem.*, **98** (1994) 964.

[20] T. Flanagan, W. Oates, *Annu. Rev. Mater. Sci.*, **21** (1991) 269.

[21] T. Flanagan, H. Noh, *Z. Naturforsch.*, **50a** (1995) 475.

[22] B. Baranowski, S. Majchrzak, T. Flanagan, *J. Phys. Chem.*, **77** (1973) 35.

[23] R. Kirchheim, *Prog. Mat. Sci.*, **32** (1988) 261.

[24] D. Wang, T. Flanagan, R. Balasubramaniam, *Scripta Mat.*, **41** (1999) 517.

[25] T. Flanagan, R. Lewis, *Trans. Faraday Soc.*, **55** (1959) 1409.

[26] E. Wicke, G. Nernst, *Ber. Bunsenges. Physik. Chem.*, **68** (1964) 224.

[27] D. Everett, P. Nordon, *Proc. Roy. Soc.*, **259A** (1960) 341.

[28] R. Defay, I. Prigogine, A. Bellemans, D. Everett, *Surface Tension and Adsorption*, Wiley, New York, 1966.

[29] D. Shashkov, M. Chisholm, D. Seidman, *Acta Mat.*, **47** (1999) 3939.

[30] D. Shashkov, D. Müller, D. Seidman, *Acta Mat.*, **47** (1999) 3953.

[31] B. Krakauer, D. Seidman, *Acta Mat.*, **46** (1998) 6145.

[32] R. Lüke, J. Bankmann, P. Wilbrandt, W. Erfurth, R. Kirchheim, *Scripta Mat.*, **39** (1998) 73.

Figure Captions

Fig. 1. SEM of an internally oxidized/reduced $Pd_{0.90}Rh_{0.10}$ alloy showing Pd nodules which have formed at the surface and the intergranular cracking.

Fig. 2. Bright field TEM of a $Pd_{0.97}Rh_{0.03}$ alloy: (*a*) internally oxidized at1073 K, 72 h; (*b*) same alloy as (*a*) after reduction.

Fig. 3. Internal oxidation of a $Pd_{0.97}Rh_{0.03}$ alloy at 1098 K plotted as % internal oxidation against $\sqrt{t}$.

Fig. 4. Rates of H_2 absorption along the plateau (323 K) for Pd and several internally oxidized *Pd*-Rh alloys and an internally oxidized $Pd_{0.97}Rh_{0.03}$ alloy. ×, Pd; ○, internally oxidized $Pd_{0.97}Rh_{0.03}$ alloy; ●, cycled internally oxidized $Pd_{0.97}Rh_{0.03}$ alloy. The following are rates for uncycled internally oxidized alloys: ▽, $Pd_{0.90}Rh_{0.10}$ alloy; □, $Pd_{0.95}Rh_{0.05}$ alloy and △, $Pd_{0.97}Rh_{0.03}$ alloy.

Fig. 5. Dilute phase absorption isotherms for unoxidized, well-annealed *Pd*-Rh alloys (323 K) where the numbers on the isotherms are the atom fractions of Rh.

Fig. 6. Isotherms for unoxidized, well-annealed *Pd*-Rh alloys (323 K). ▽, Pd-H; dashed line absorption plateau for $Pd_{0.99}Rh_{0.01}$; □, $Pd_{0.97}Rh_{0.03}$; △, $Pd_{0.95}Rh_{0.05}$; ○, $Pd_{0.90}Rh_{0.10}$. ◊, $Pd_{0.90}Rh_{0.10}$ alloy after exposure to the atmosphere at 1273 K, 24 h. The empty and filled symbols are for absorption and desorption, respectively. The inset shows the plateau pressures as a function of X_{Rh}.

Fig. 7. Dilute phase isotherms for an internally oxidized $Pd_{0.97}Rh_{0.03}$ alloy (323 K). ○, well-annealed; dashed curve, Pd; △, internally oxidized (1073 K, 120 h)/reduced; □, cycled.

Fig. 8. Dilute phase isotherms for the internally oxidized $Pd_{0.95}Rh_{0.05}$ alloy (323 K) compared to Pd and an unoxidized $Pd_{0.95}Rh_{0.05}$ alloy. ○, Unoxidized $Pd_{0.95}Rh_{0.05}$ alloy; dashed curve, Pd; △, internally oxidized (1073 K, 120 h)/reduced $Pd_{0.95}Rh_{0.05}$ alloy; ▲, repeat measurement of internally oxidized $Pd_{0.95}Rh_{0.05}$ alloy after evacuation at 323 oK for 2 h; □, cycled internally oxidized $Pd_{0.95}Rh_{0.05}$ alloy; ■, repeat measurement of cycled internally oxidized $Pd_{0.95}Rh_{0.05}$ alloy after evacuation at 323 K for 2 h.

Fig. 9. Dilute phase isotherms for the internally oxidized (1093 K, 120 h) $Pd_{0.90}Rh_{0.10}$ alloy (323 K) before and after annealing *in vacuo* at various temperatures. Dashed curve, Pd; ○, internally oxidized $Pd_{0.90}Rh_{0.10}$ alloy; □, internally oxidized $Pd_{0.90}Rh_{0.10}$ alloy evacuated/annealed at 323 K, 2 h; ▽, internally oxidized $Pd_{0.90}Rh_{0.10}$ alloy evacuated/annealed at 373 K, 2 h; ▲, evacuated/ annealed at 403 K, 2 h; ×, evacuated/annealed at 453 K, 2 h; △, evacuated/annealed at 473 K, 2 h; ●, evacuated/annealed at 503 K, 2 h.

Fig. 10. Dilute phase isotherms for the internally oxidized $Pd_{0.90}Rh_{0.10}$ alloy (323 K). ○, Well-annealed alloy; dashed curve, Pd; ●, $Pd_{0.90}Rh_{0.10}$ alloy exposed to the atmosphere at 1273 K, 24 h; △, internally oxidized (1073 K, 120 h)/reduced alloy; ▽, internally oxidized alloy evacuated/ annealed at 673 K, 2 h; ▼, internally oxidized alloy evacuated/annealed at 773 K, 2 h; □, internally oxidized alloy evacuated/annealed at 873 K, 2 h.

Fig. 11. Complete isotherms for the $Pd_{0.97}Rh_{0.03}$ alloy (323 K) after internal oxidation (1073 K, 120 h)/reduction. Dashed lines, Pd; ○, unoxidized alloy; △, internally oxidized alloy. Empty and filled symbols are for absorption and desorption, respectively.

Fig. 12. Complete isotherms for the $Pd_{0.95}Rh_{0.05}$ alloy (323 K) after internal oxidation (1073 K, 120 h)/reduction. Dashed lines, Pd; ○, unoxidized alloy; △, internally oxidized $Pd_{0.95}Rh_{0.05}$ alloy; □, cycled internal oxidation $Pd_{0.95}Rh_{0.05}$ alloy. Empty and filled symbols are for absorption and desorption, respectively.

Fig. 13. Complete isotherms for the $Pd_{0.90}Rh_{0.10}$ alloy (323 K) after internal oxidation (1073 K, 120 h)/reduction. Dashed lines, Pd; ○, internally oxidized (1073 K, 120 h) $Pd_{0.90}Rh_{0.10}$ alloy; △,

internally oxidized (1073 K, 120 h) $Pd_{0.90}Rh_{0.10}$ alloy annealed at 873 K, 2 h; ▽, fifth cycle for the internal oxidation (1073 K, 120 h) $Pd_{0.90}Rh_{0.10}$ alloy; □, internally oxidized (1073 K, 120 h) $Pd_{0.90}Rh_{0.10}$ alloy annealed at 873 K, 20 h. Empty and filled symbols are for absorption and desorption, respectively.

Fig. 14. Hysteresis scans for the $Pd_{0.97}Rh_{0.03}$ alloy (323 K) after internal oxidation (1073 K, 144 h)/reduction. ○, Initial isotherm after internal oxidation of $Pd_{0.97}Rh_{0.03}$ alloy; ▽, second isotherm for internally oxidized $Pd_{0.97}Rh_{0.03}$ alloy; □, absorption scan started at A; △, absorption scan started at B. The dashed lines without symbols are for Pd. Empty and filled symbols are for absorption and desorption, respectively.

Fig. 15. Hysteresis scans for the $Pd_{0.90}Rh_{0.10}$ alloy (323 K) after internal oxidation (1073 K, 144 h)/reduction. ○, Initial isotherm after internal oxidation of $Pd_{0.90}Rh_{0.10}$ alloy; ▽, second cycle for internally oxidized $Pd_{0.90}Rh_{0.10}$ alloy; □, absorption scan started at A; △, absorption scan started at B. The dashed lines without symbols are for Pd. Empty and filled symbols are for absorption and desorption, respectively.

Fig. 16. Hysteresis scans for the $Pd_{0.90}Rh_{0.10}$ alloy (323 K) after internal oxidation (1073 K, 144 h)/reduction and annealing at 873 K for 20 h. ○, internal oxidation and evacuation/annealing at 873 K of $Pd_{0.90}Rh_{0.10}$ alloy; ▽, second cycle for internally oxidized $Pd_{0.90}Rh_{0.10}$ alloy; □, absorption scan started at A; △, absorption scan started at B. The dashed lines without symbols are for Pd. Empty and filled symbols are for absorption and desorption, respectively.

Fig. 1.

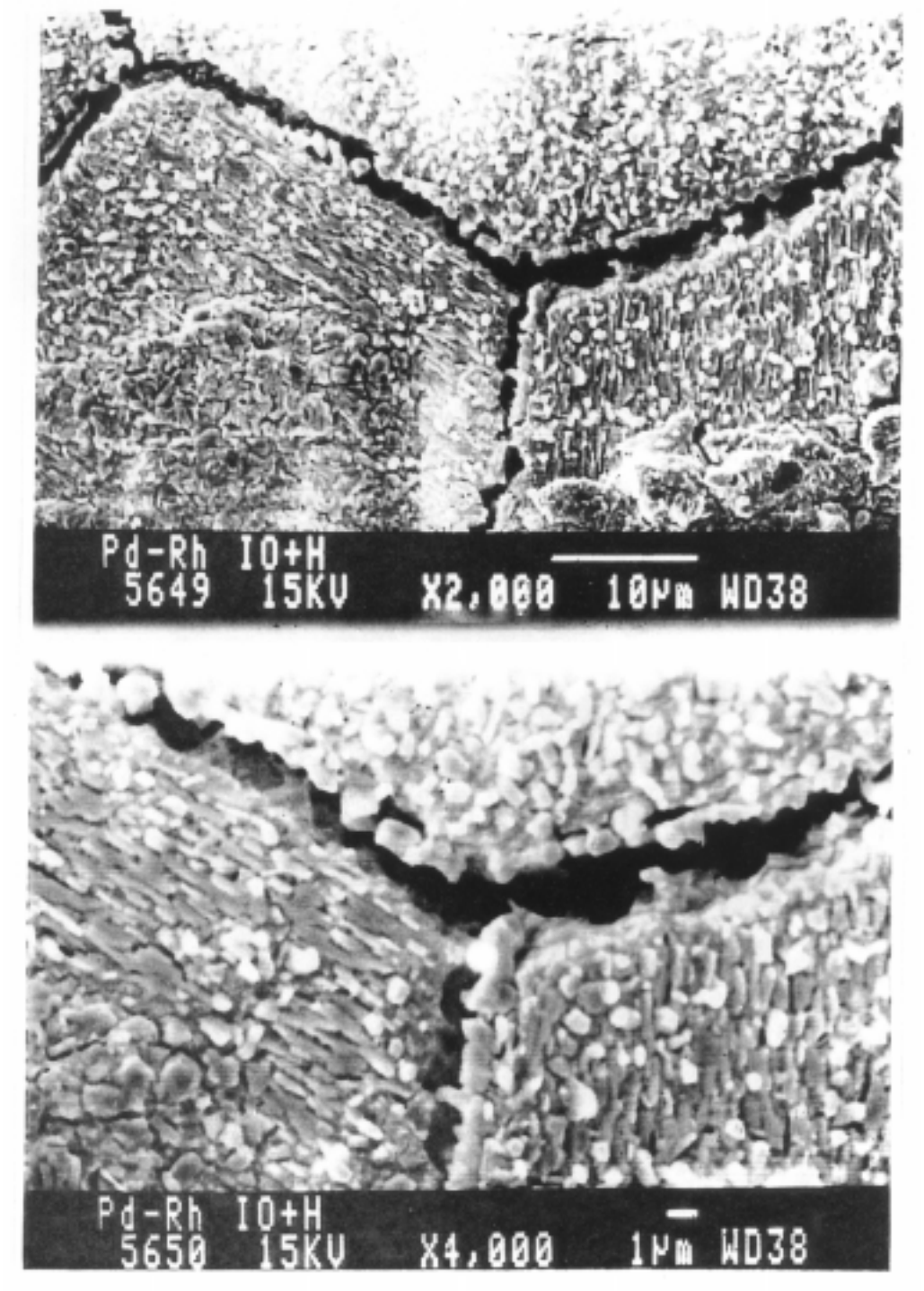
Pd-Rh IO+H
5649 15KV X2,000 10µm WD38
Pd-Rh IO+H
5650 15KV X4,000 1µm WD38

Fig. 2.

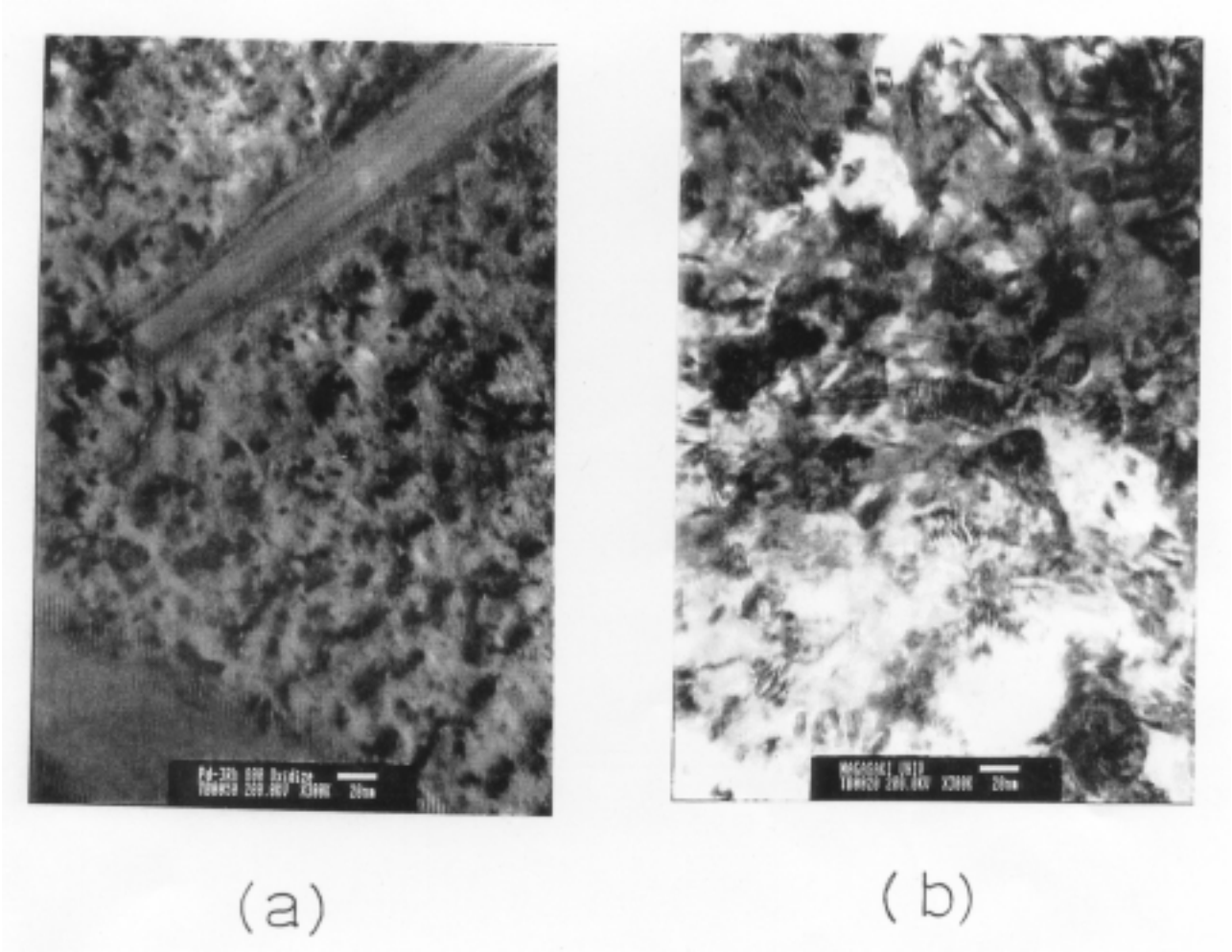

Fig. 3.

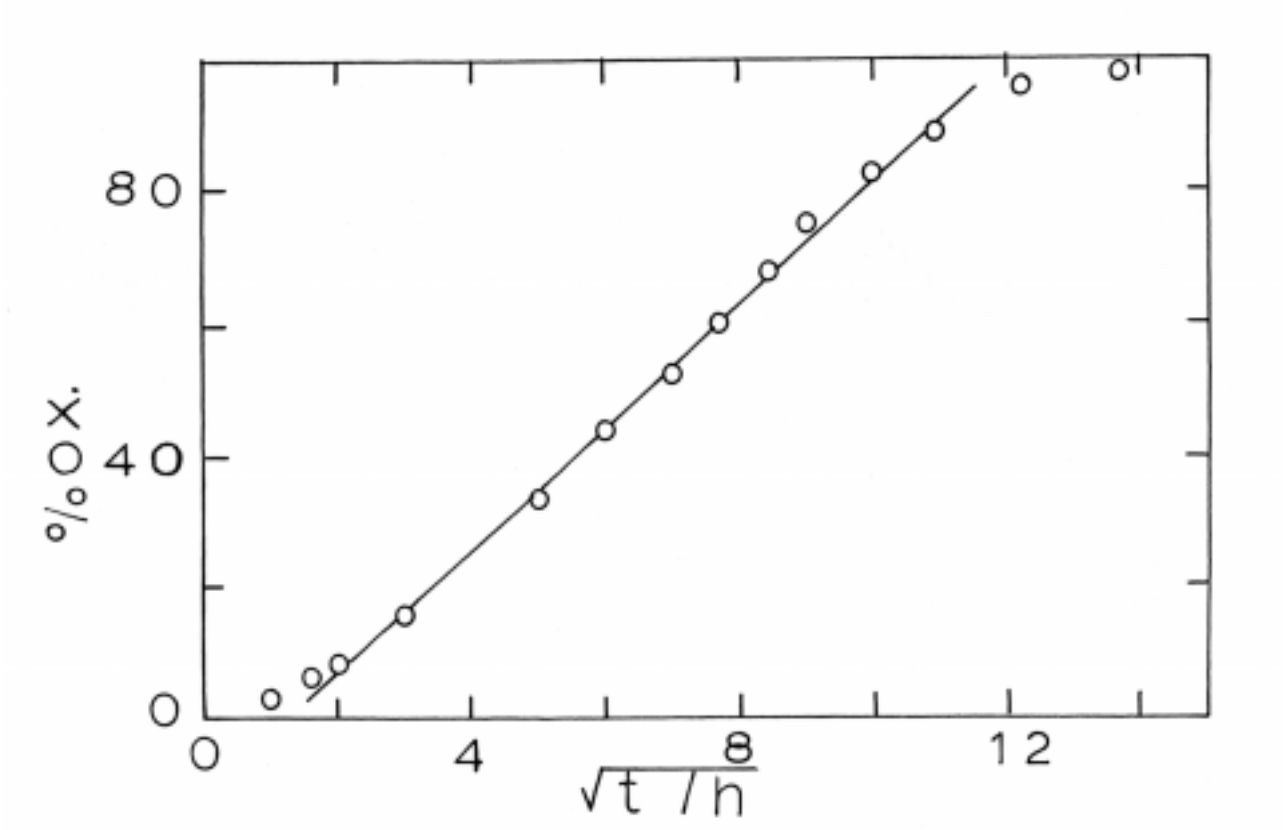

Fig. 4.

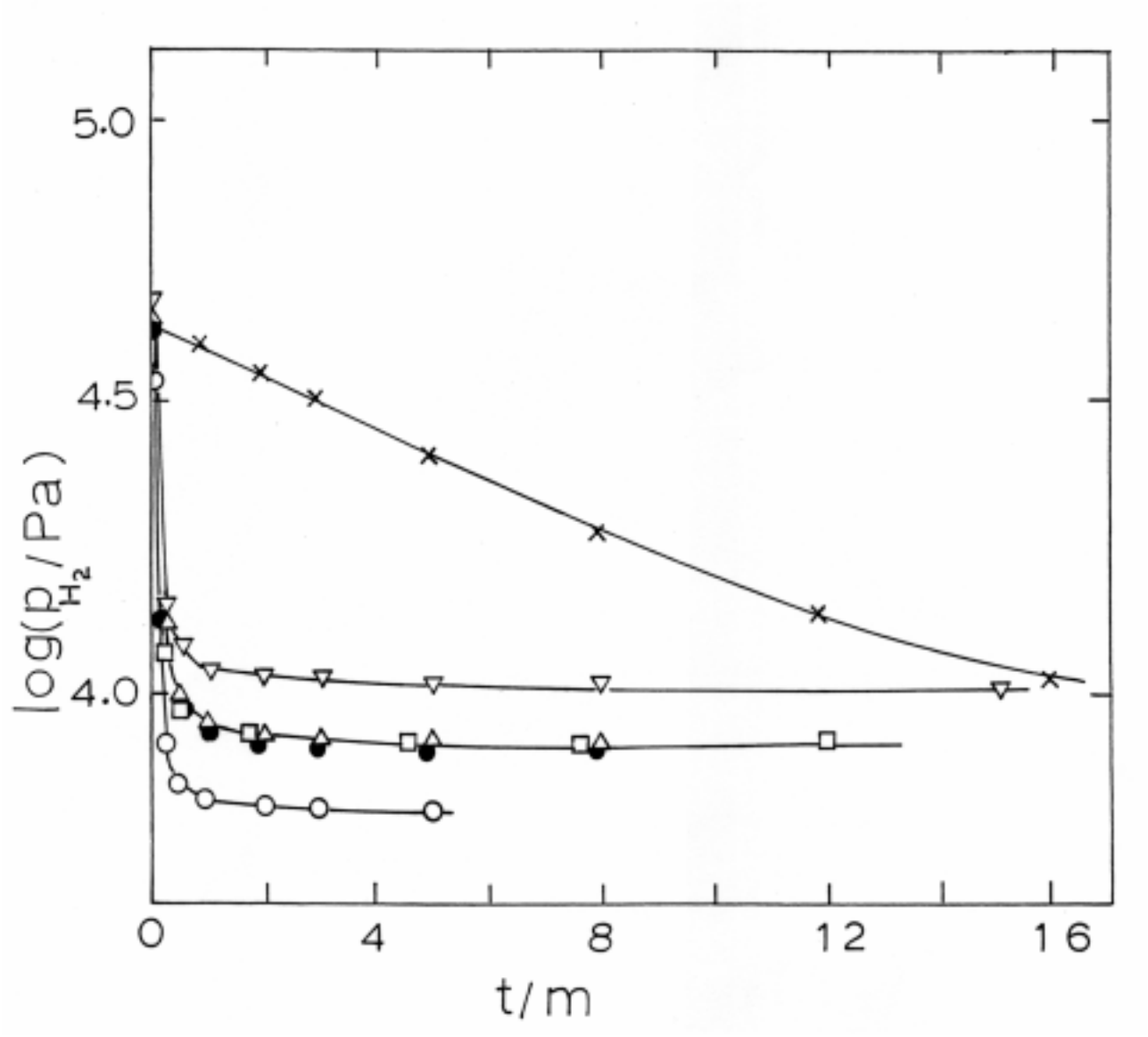

Fig. 5.

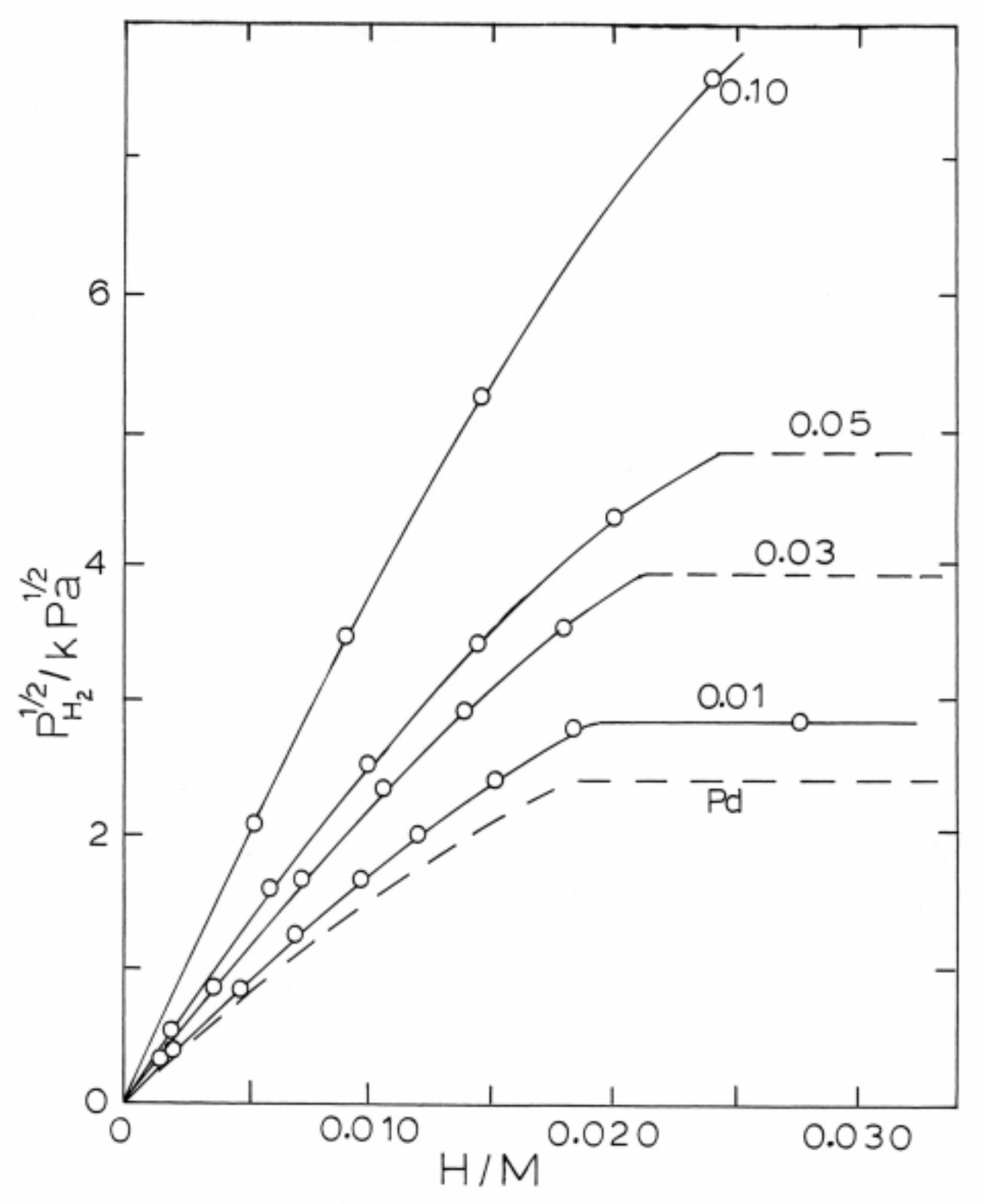

Fig. 6.

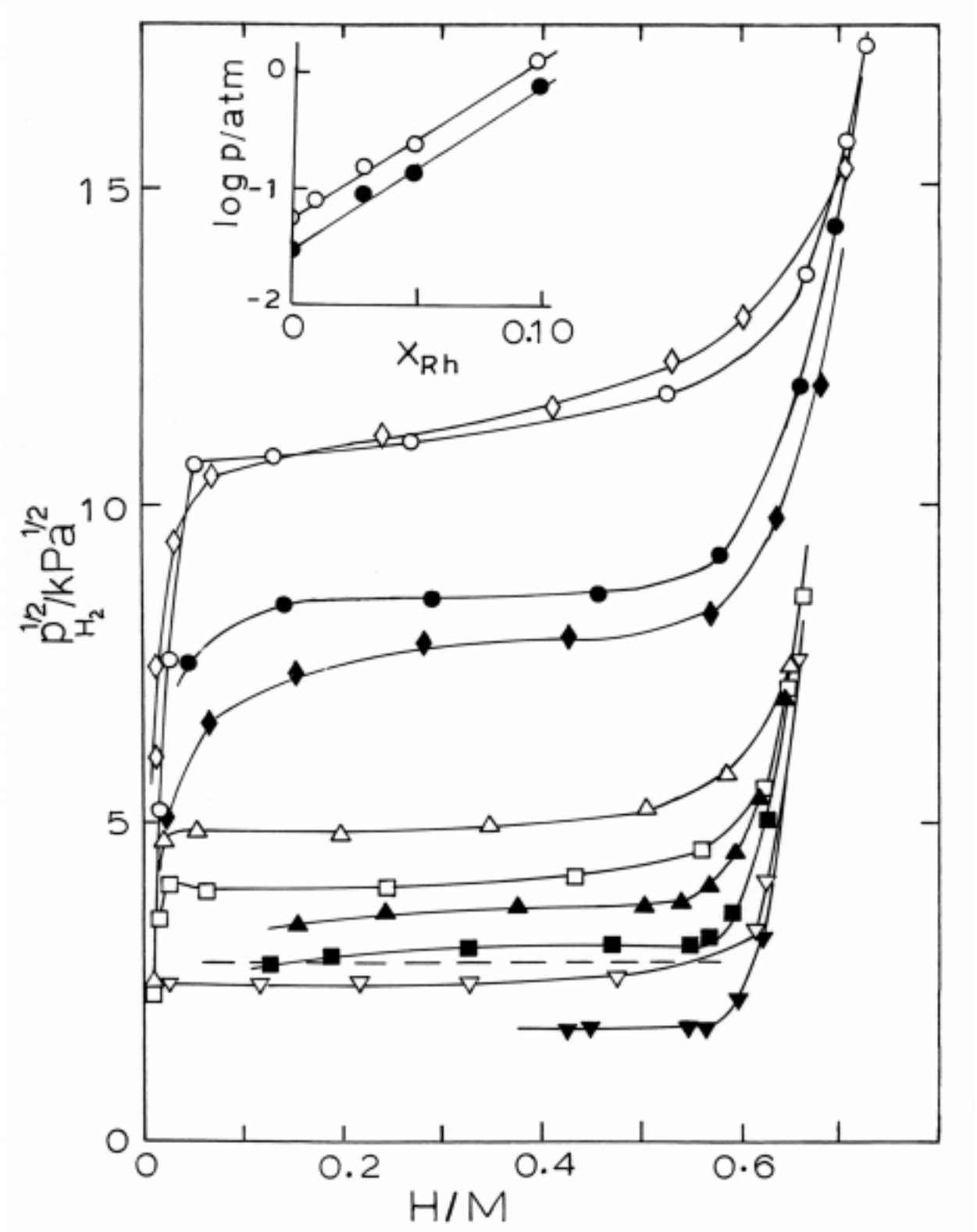

Fig. 7.

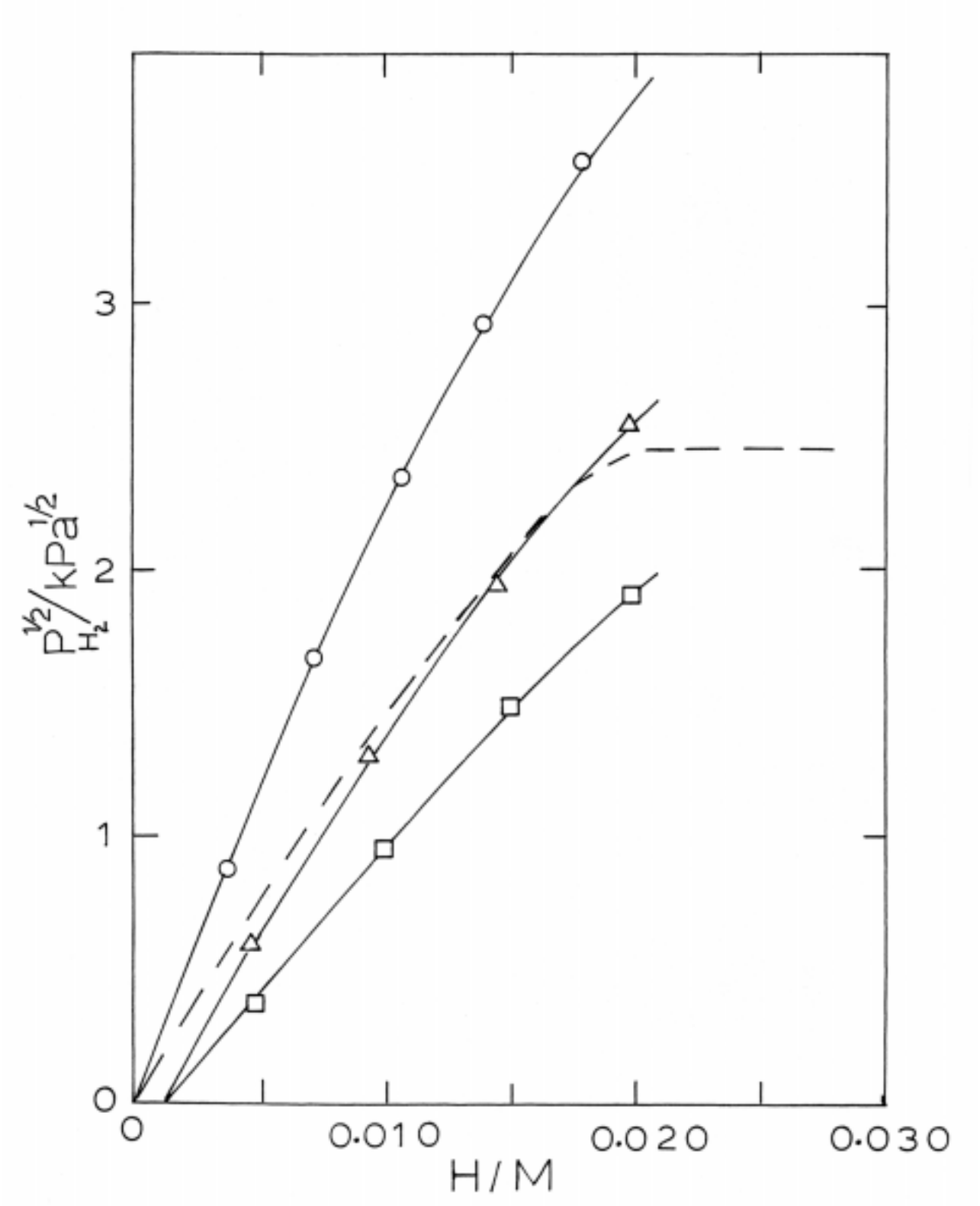

Fig. 8.

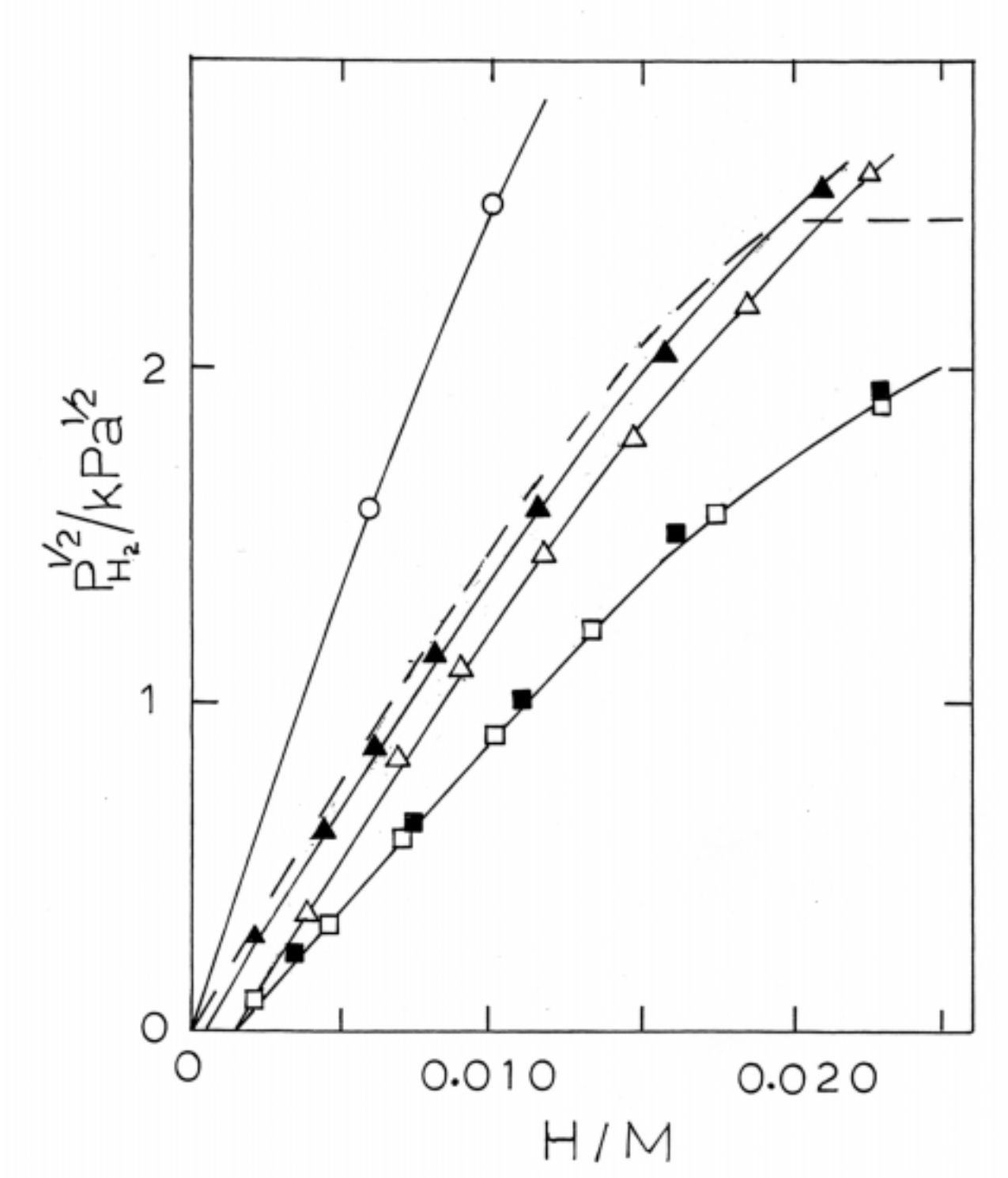

Fig. 9.

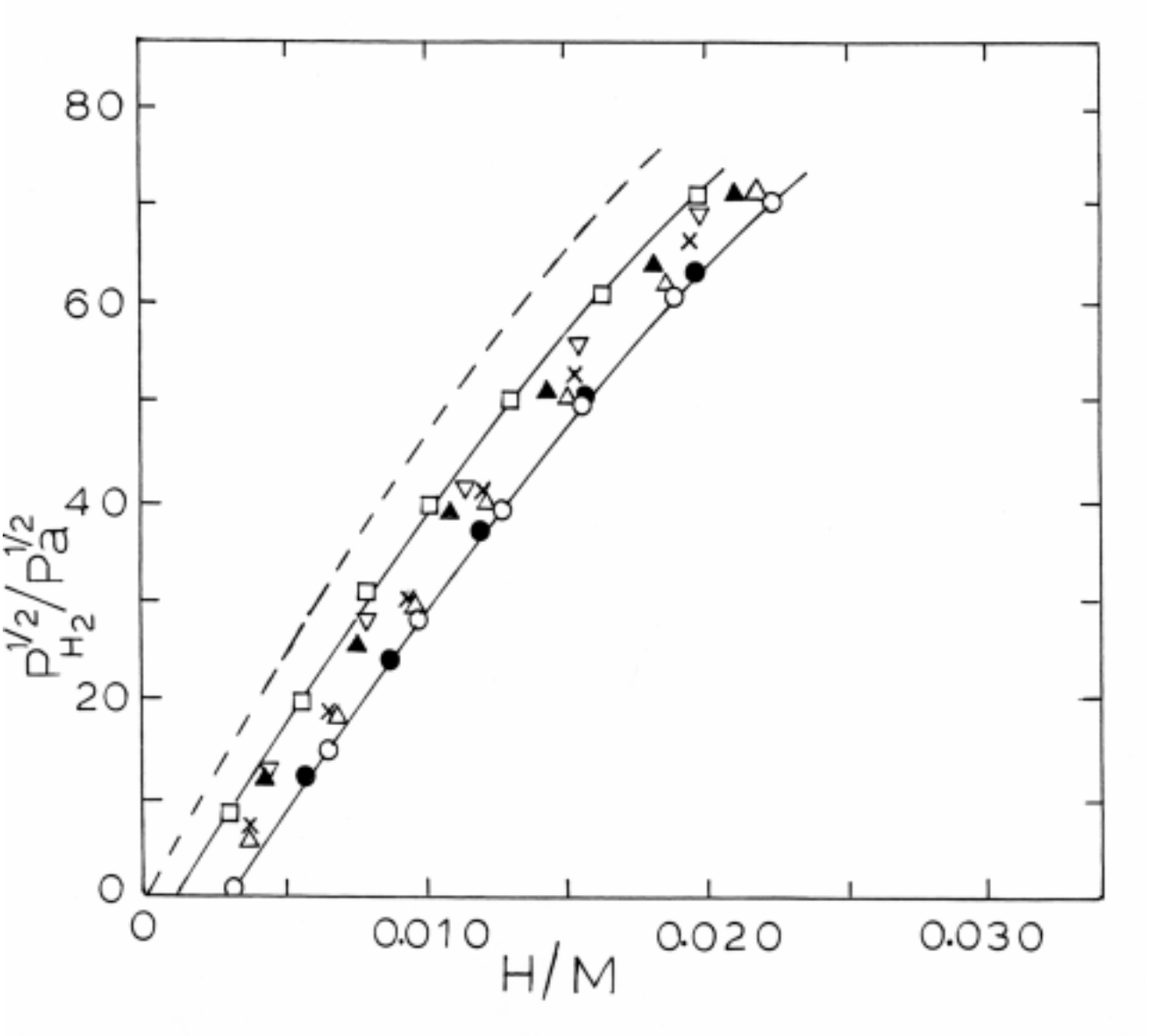

Fig. 10.

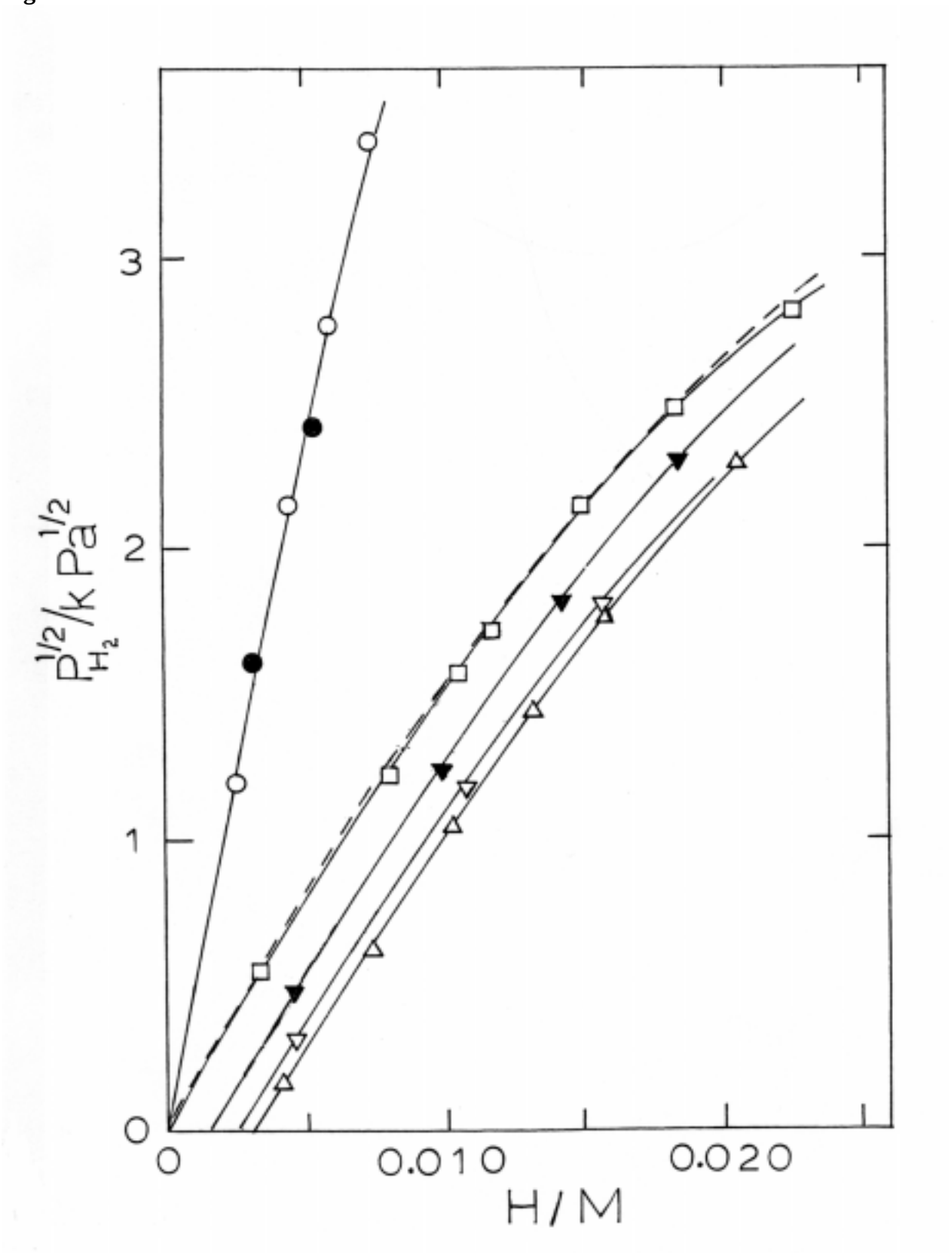

Fig. 11.

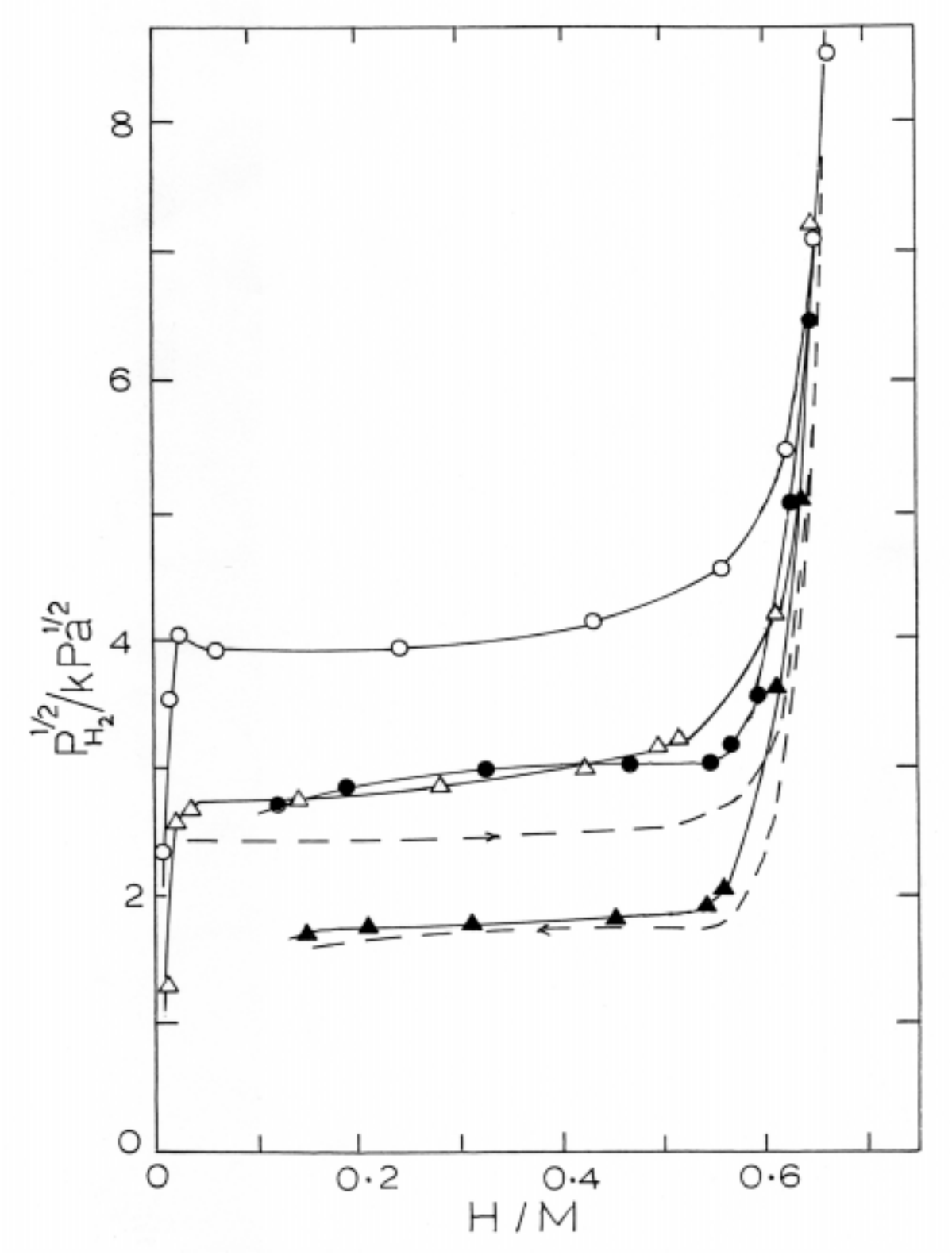

Fig. 12.

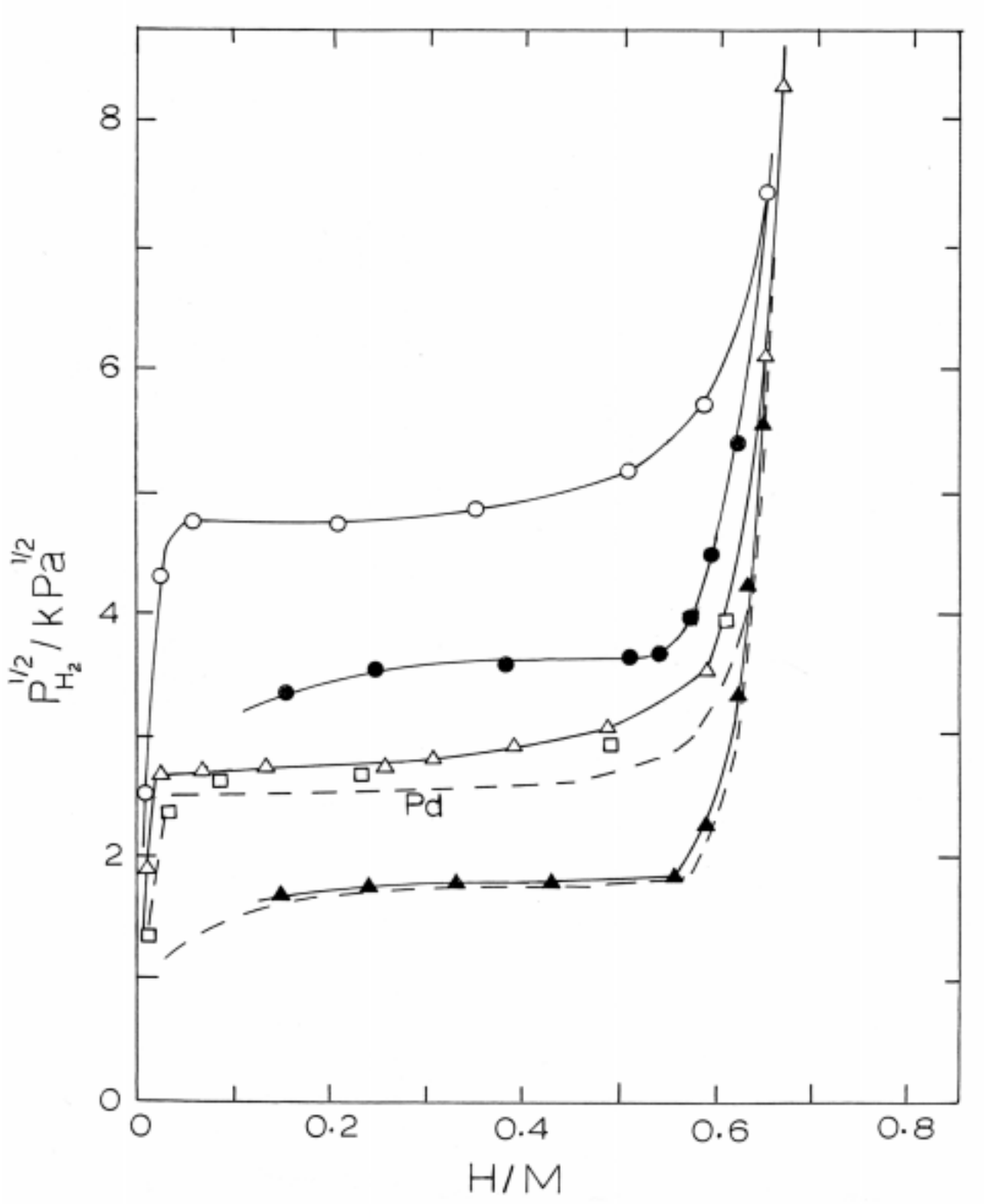

Fig. 13.

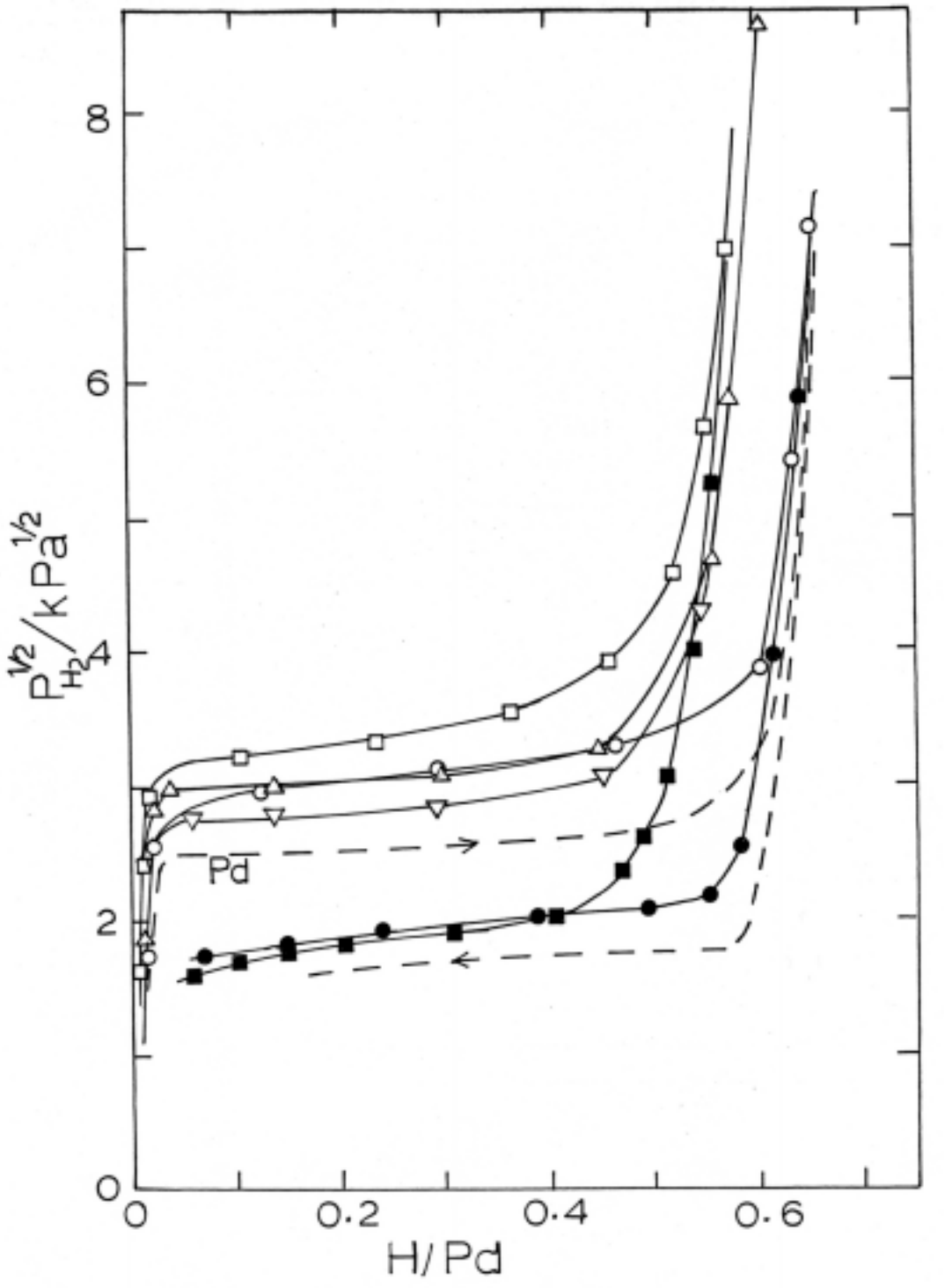

Fig. 14.

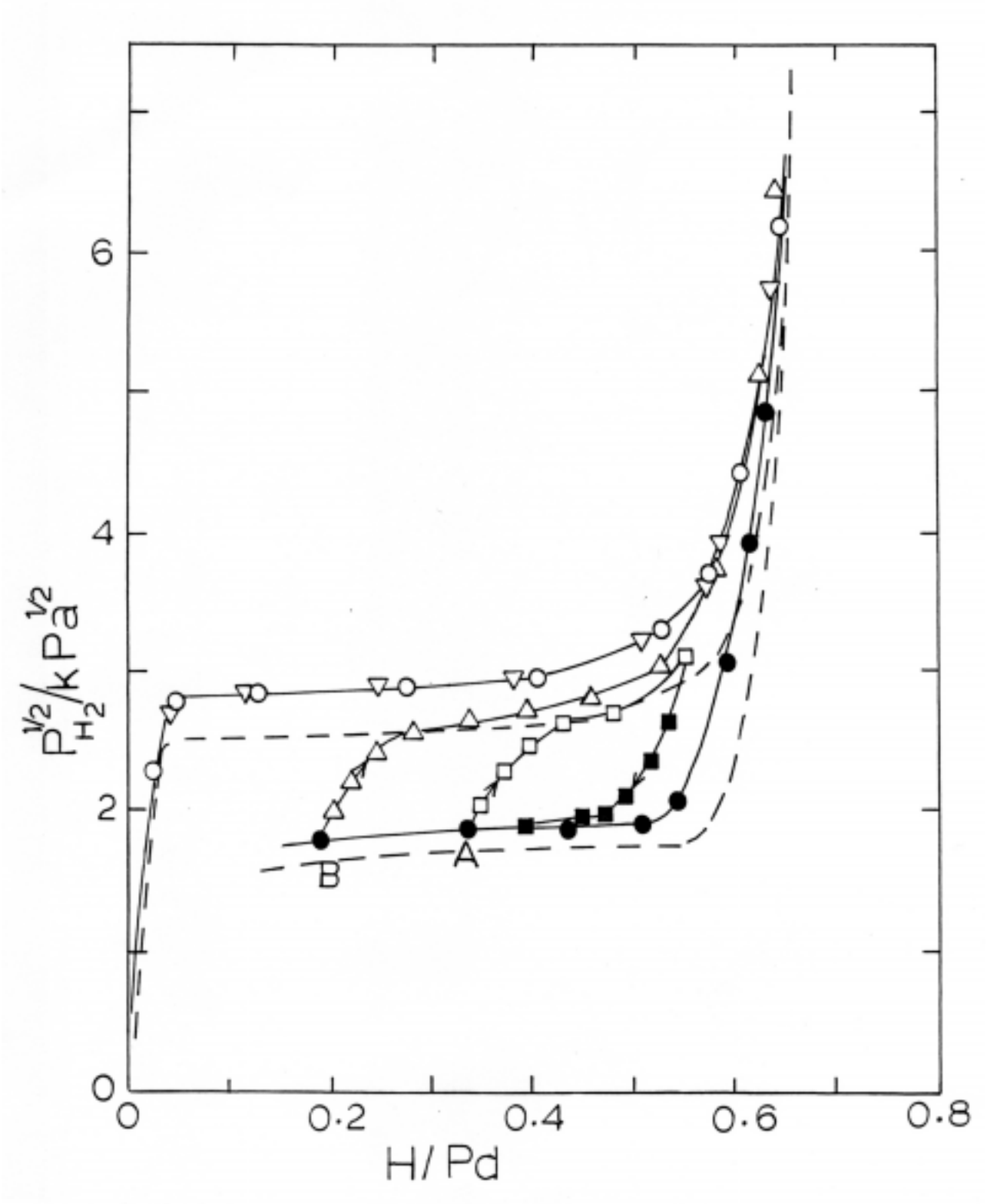

Fig. 15.

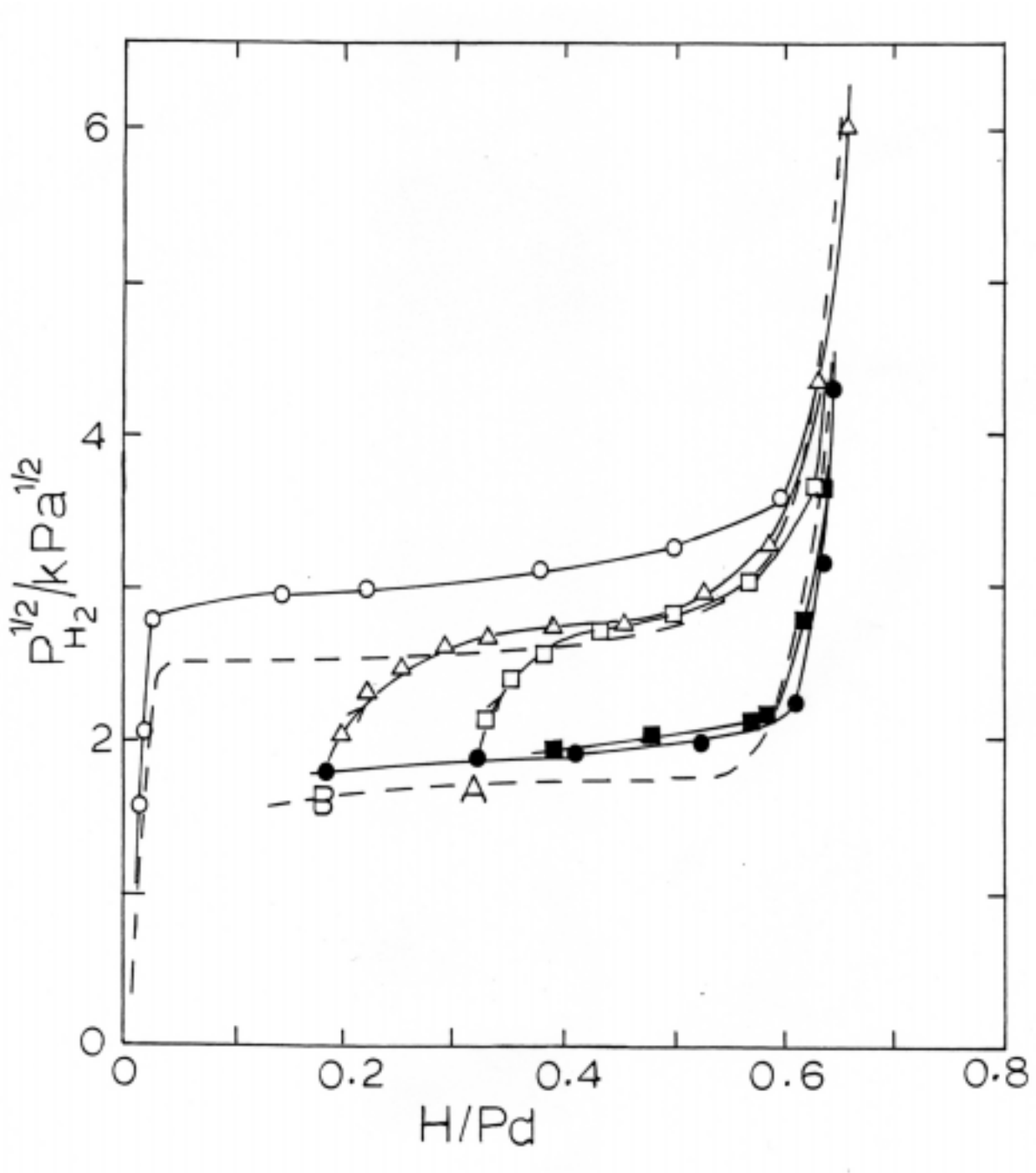

Fig. 16.